Antisense Oligonucleotide technologies for neuronal cell regeneration after spinal cord injury

Artur Guilherme Machado de Lima Costa

Dissertação de Mestrado em Bioquímica

Universidade do Porto
Faculdade de Ciências
Instituto de Ciências Biomédicas Abel Salazar

2013

Artur Guilherme Machado de Lima Costa

Antisense Oligonucleotide technologies for neuronal cell regeneration after spinal cord injury

Dissertação de Candidatura ao grau de Mestre em Bioquímica da Universidade do Porto

Orientador – Doutor Pedro Moreno
Categoria – Investigador Assistente
Afiliação – Instituto de Engenharia Biomédica, Porto
Co-orientador – Doutora Ana Paula Pêgo
Categoria – Investigador Principal
Afiliação – Instituto de Engenharia Biomédica, Porto

2013

FACULDADE DE CIÊNCIAS DA UNIVERSIDADE DO PORTO

ANTISENSE OLIGONUCLEOTIDE TECHNOLOGIES FOR NEURONAL CELL REGENERATION AFTER SPINAL CORD INJURY

Artur Guilherme Machado de Lima Costa
BSc in Biochemistry
from Faculdade de Ciências da Universidade do Porto

Master's thesis in Biochemistry

Done under the supervision of
Pedro Moreno, PhD, and Ana Paula Pêgo, PhD

Porto, September 2013

Abstract

Spinal cord injury is a serious clinical problem, since it does not spontaneously heal and frequently leads to paralysis, leading to severe health, economic and social consequences to both patients and their families. Neurons have low potential for regeneration and the lesion site environment severely hinders the formation of neurite extensions, essential for the reestablishment of neuronal connections. Among the reported events, a pathway featuring several myelin inhibitors as well as a common downstream regulator was identified as having a major role limiting neurite formation. A gene therapy approach is likely able to target the inhibitory genes, at lower dosage and dose frequency than conventional pharmacotherapy, and with fewer side effects. However, low stability on bodily fluids and low cellular internalization of nucleic acids raise the need for a vector.

Antisense oligonucleotides (AON) were used to induce RNase H-mediated degradation of target mRNA sequences. These codify for myelin inhibitors-activated proteins, namely RhoA from the Rho family of small GTPases and Glycogen Synthase Kinase 3β (GSK3β). AON sequences were defined based on target sequence availability, binding affinity and specificity, then tested *in vitro* in cell cultures. A commercial transfection reagent was used to ensure transfection efficiency during activity studies, although safety and specificity issues discourage its use for *in vivo* applications. Gene downregulation was determined by reverse transcription-polymerase chain reaction.

Aiming for *in vivo* delivery of AONs, a chitosan-derived biomaterial was developed in order to bind AON and deliver them to target cells. Trimethylchitosan is not dependent on pH for solubility and binding stability since the trimethyl substituent ensures permanent positive charge at most pH values. Theoretically, electrostatic interactions are sustained at physiological conditions. Additionally, hydrophobic moieties, which were expected to improve AON binding properties, cell membrane interaction and lysosomal escape, were also tested. Particle size, chitosan-AON binding properties, cellular binding and uptake were analyzed.

The tested AON sequences were successful in downregulating the target mRNA, at optimum transfection conditions with the commercial reagent. Unmodified TMC was not able to mediate efficient transfection and required high N/P ratios to produce stable TMC-AON interaction; Stearic acid-modified TMC, on the other hand, showed improved AON binding properties and was able to transfect cells at high N/P ratios.

The work was developed in the context of a larger project, and included the cooperation of teammates, *e.g.* in the biomaterial synthesis, target protein characterization. This study was conducted in the context of the project “Characterization of Cell-intrinsic axonal regeneration determinants and their use to promote repair after CNS injury”, funded by grant HMSP-ICT/0020/2010 from FCT (Fundação para a Ciência e Tecnologia).

Table of contents

List of Abbreviations

AON	Antisense oligonucleotide
cAMP	Cyclic Adenosine monophosphate
CNS	Central Nervous System
CQ	Chloroquine
CLASP2	Cytoplasmic linker-associated protein 2
DMEM	Dulbecco's Modified Eagle Medium
EDTA	Ethylenediaminetetraacetic acid
GSK3β	Glycogen Synthase Kinase 3β
GDI	Guanine Dissociation Inhibitor
GPI	Glycosylphosphatidylinositol
HEPES	4-(2-Hydroxyethyl)piperazine-1-ethanesulfonic acid
HKR	HEPES-Krebs-Ringer solution
LNA	Locked Nucleic Acid
MAG	Myelin-associated glycoprotein
MAI	Myelin-associated inhibitors
MT	Microtubules
NgR	Nogo Receptor
NP	Nanoparticle
N/P ratio	Ratio of polymer amines to nucleic acid phosphates
OMgp	Oligodendrocyte-myelin Glycoprotein
SCI	Spinal Cord Injury
PBS	Phosphate buffered saline
PCR	Polymerase Chain Reaction
PEG	Polyethylene glycol coating
PS	Phosphoriothioate nucleotide modification
RT-PCR	Reverse Transcription Polymerase Chain Reaction
TAE	Tris-Acetic acid-EDTA solution
TBE	Tris-Boric acid-EDTA solution
T_m	Melting temperature (nucleic acid interaction)
TMC	Trimethylchitosan

List of Figures

Introduction

Spinal Cord Injury

Acute traumatic spinal cord injury (SCI) occurs worldwide with an estimated annual incidence of 130'000 and is associated with severe physical, psychological, social and economic burdens on patients and their families[1, 2]. As the central nervous system (CNS) does not spontaneously regenerate, paralysis is a common occurrence after SCI. Regeneration may be achieved by re-establishing the neuronal connections via neurite outgrowth; however, it is conditioned by several factors, such as remaining regeneration substrate, length of the lesion site, glial scar formation, inflammatory response, lack of neurotrophic support, and most importantly, an abundance of glial (ephrins, semaphorins[3]), myelin (MAG, OMgp, Nogo[4]) and extracellular matrix inhibitors (chondroitin sulfate proteoglycans[5]). The abundance of inhibitory molecules that limits neuronal plasticity is related to circuit maturation during development of higher vertebrates, evidenced by lower vertebrates like the gecko or the newt that are able of some spontaneous neuronal regeneration[6, 7].

Nogo, oligodendrocyte-myelin glycoprotein (OMgp) and myelin-associated glycoprotein (MAG) are myelin-associated inhibitors (MAI) present in myelin sheaths and have major importance in the inhibition of neuronal regeneration. Mechanical injury to myelinated fibers leads to the release of these molecules. Nogo66, a Nogo domain, as well as OMgp and MAG, have been shown to bind to Nogo receptor (NgR)[8]. NgR is a glycosylphosphatidylinositol (GPI)-anchored protein present on the outer leaflet of the plasma membrane. Cleavage of that anchor by phospholipase C, NgR antibody targeting[9] or NgR antisense downregulation[10] have been shown to lead to the abolition of growth cone collapse induced by myelin inhibitors. The same effect may be achieved by a small fragment of the Nogo66 domain, a highly efficient peptide antagonist named NEP1-40[11]. The receptor complex formed after ligand binding also includes $p75^{NTR}$ and Lingo -1. The former was identified as responsible for signal transduction, but Lingo-1 was only recently discovered and is still yet to be characterized. $p75^{NTR}$ acts as a transducer for NgR signaling by releasing RhoA from its interaction with RhoA-GDI (Rho guanine dissociation inhibitor) and enabling its activation by GDP to GTP substitution[8]. Similarly, chondroitin sulfate proteoglycans and chemorepulsive guidance molecules also activate RhoA, thus inhibiting neurite outgrowth[12].

RhoA

RhoA belongs to the Rho family of small GTPases, and has a major role on regulating actin

cytoskeleton dynamics. Rho kinases alternate between an active GTP-bound state and an inactive GDP-bound state. GDP to GTP substitution is catalyzed by guanine exchange factors (GEF), whereas GTP degradation to GDP is facilitated by GTPase activating proteins (GAP)[3]. Association with GDP dissociation inhibitor (GDI) maintains Rho in its inactive GDP-bound form. While the two other major Rho kinases, Rac and Cdc42, respond to attractive guidance cues and promote actin polymerization, RhoA activation by negative cues leads to actin depolymerization [13].

RhoA is involved in MAI-induced inhibition of axon regeneration[14]. Higher GTP-RhoA levels, associated with activated RhoA, have been reported in the presence of inhibitory molecules and siRNA-mediated silencing of RhoA was shown to promote neurite outgrowth[10, 15]. RhoA is inactivated when cAMP levels are raised, *e.g.* in the presence of growth factors; inactivation is suggested to occur by dissociation of the NgR signaling complex, mediated by cAMP-activated Protein Kinase A[8].

Rho-associated coiled-coil-containing protein kinase (ROCK) is a well characterized Rho downstream effector. It is activated when Rho binds to the Rho binding domain (RBD), interfering with the interaction between the catalytic domain and autoinhibitory region. Inhibiting ROCK leads to enhanced branching and axon elongation[16], and also inhibits its activator[17].

Glycogen Synthase Kinase 3β

Previous studies in the project "Characterization of Cell-intrinsic axonal regeneration determinants and their use to promote repair after CNS injury", in which the work developed in this master thesis was integrated, have identified another key component of inhibitory signaling pathways that limit neuronal regeneration after SCI, Glycogen Synthase Kinase 3 β (GSK3β).

Glycogen Synthase Kinase 3 (GSK3) was first discovered to regulate glycogen metabolism regulation, and many other roles have been identified since. There are more than 60 reported substrates[18], *i.e.* this kinase is involved in several cellular processes, like cell cycle, apoptosis and cytoskeleton dynamics. It is usually active under normal resting conditions and is subject to many regulation pathways in order to selectively target its substrates. One of the best characterized mechanisms is phosphorylation at Ser9 by the phosphatidylinositol 3-kinase (PI3K)/Protein kinase B signaling pathway: PI3K activates PK_B in response to insulin, which phosphorylates and inhibits GSK3 at Ser9 [19, 20]. Conversely, Tyr216 phosphorylation results in activation.

There are two mammalian isoforms of Glycogen Synthase Kinase 3, of which β (57 kDa) is more abundant in the CNS and relevant for this work than α (52 kDa). Among GSK3β functions,

stabilizing microtubules (MT) by phosphorylating MT-associated proteins[21] is especially pertinent, they are necessary for neurite outgrowth. Cytoplasmic linker associated protein 2 (CLASP2), one of GSK3β substrates, binds to the plus end of MT or to MT lattices, and regulates MT stabilization [22]. At low activity levels, CLASP2 is incapable of stabilizing MT polymerization, and both binding modes are compromised. At intermediate activity levels, CLASP2 selectively binds to the MT plus ends and promotes their extension. At high activity levels, CLASP2 binds to both the plus ends and MT lattices, enabling polymerization but also looping (fig. 1).

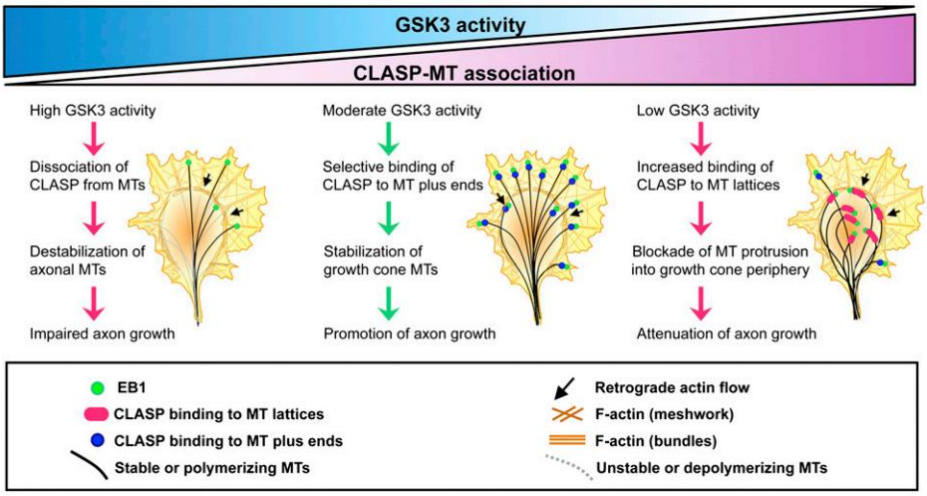

Figure 1 – **GSK3 activity influence on CLASP-MT association**[22]. Moderate GSK3 activity promotes axon growth, since it secures CLASP2 MT stabilizing effects and does not trigger CLASP2-induced MT looping.

The induction of GSK3β activity after SCI is linked to lower MT stability. As explored below, several drugs have been used to downregulate GSK3β and have been successful in remyelinization and neurite extension [23, 24], although there are contradictory perspectives that propose that MAI inhibits GSK3β [25]. Nonetheless, low inhibition seems the best approach towards neuronal regeneration.

Therapeutic Strategies

Currently used therapeutic approaches to SCI have limited success [1 2], but intensive research on the matter has begun to show practical results. New approaches, under development or on clinical trials, are identified bellow. The following summary focuses on inhibiting negative regulators of neuronal regeneration.

With the identification of Nogo as an important component of MAI-dependent inhibitory pathways of neuronal regeneration, targeting Nogo neutralization became clinically relevant. IN-1, an anti-Nogo antibody, has been shown to promote axon regeneration in many regions of the CNS. Nonetheless, Nogo is just one of the NgR ligands, and compensatory upregulation of the remaining may hinder therapeutic application of Nogo inhibition. On the other hand, NgR may be targeted by NEP1-40, and promising results on regeneration after spinal cord injury and functional recovery have been reported[26, 27]. $p75^{NTR}$, although it is also part of the receptor complex, is not a valid target, since it participates in a vast range of transmembrane signaling pathways, including those of neurotrophins such as nerve growth factor (NGF) and brain-derived neurotrophic factor (BDNF).

Rho and Rho-associated kinase (ROCK) are popular targets in neuronal regeneration therapies, as this pathway is crucial to NgR downstream signaling. Y27632 is a specific inhibitor of ROCK, abolishing its negative effects on growth cones, and has been shown to sustain nerve regeneration. However, it is dependent on cAMP levels, related to the intrinsic neuronal growth ability and/or the presence of growth factors [14]. The C3 transferase exoenzyme from *Clostridium botulinum* is another Rho inhibitor, and also has neuronal regenerative effects [8]. The major obstacle to the use of C3 in a clinical context is lack of membrane permeability[13], which has been tentatively addressed by conjugation with cell-penetrating peptides (explored below)[28]. However, discrepancies between *in vitro* and *in vivo* results are significant, probably due to technical issues, *e.g.* improper doses, pharmacokinetics and insufficient drug uptake by relevant cells[29]. Fasudil is one of the few clinically available Rho inhibitors to date[3, 30], and has shown much better results than Y27632 and C3; it may have a mechanism other than targeting RhoA [31, 32].Conjugation approaches , *e.g.* drugs and growth factor-producing bone marrow stromal cells (BMSC), have shown synergistic effects[33]. Nonetheless, cell therapy is technically demanding, and may pose obstacles to clinical application.

GSK3β participates in the pathophysiology of many disorders, such as Alzheimer's Disease, schizophrenia and mood disorders[34], besides mediating MAI-induced growth cone collapse[24, 35]. Several inhibitors have been developed, but the available options are far from optimal. Despite a low selectivity, low clearance and high IC_{50}, lithium is frequently used as a mood regulator, targeting GSK3 among other proteins[34, 36]. The low selectivity and high IC_{50} are associated to its binding mechanism of competition for the Mg^{2+} binding site[19]. SB216763 and SB415286, which are also among the most used drugs against GSK3 and are more potent and specific than lithium, have off-target effects due to an ATP-binding site-competing binding mechanism. Additionally, they may cause ablation of the anti-tumorigenic role of GSK3, by inhibiting GSK3-mediated degradation of proto-oncogenes, *e.g* adenomatous polyposis coli (APC), β-catenin, cyclin D1, c-Myc, snail, Bcl-3. The discovery of new pharmacologic drugs is hindered by structural homology to other signaling

Field Code Changed

Field Code Changed

proteins, and a new drug platform with increased target specificity would be most advantageous.

As stated above, RhoA inhibition has a positive effect on the blockade of MAI-inhibitory pathways, and GSK3β inhibition provides a solution for improving MT dynamics and growth cone stabilization. Thus, a combinatorial approach inhibiting both RhoA and GSK3β is apt to provide a satisfactory synergistic effect. This study will focus on targeting both proteins, as a new therapeutic approach after SCI.

The Genetic Approach

Gene therapy has been subject of great interest since it was introduced in the scientific community, since the concept of correcting genetic pathologies by introducing therapeutic genes or replacing/deleting aberrant ones is a very promising idea. Meanwhile, the definition of gene therapy has expanded and it now broadly includes the use of gene-encoding DNA plasmids, RNA molecules or oligonucleotides to correct genetic information or regulate gene expression (fig. 2). Specifically, regulation of gene expression through oligonucleotide gene therapy is believed to have several potential advantages over conventional pharmacotherapy, such as fewer side effects (derived from higher specificity), a broader set of available targets and easier design. In the context of antisense oligonucleotide therapies, explored below, an analogy to traditional pharmacology can be made: target mRNA may be considered as the receptor, and the antisense sequence as the drug. The specific approach of antisense therapy yields another advantage, since recycling of the degradation complex sustains activity for a much longer period than traditional drugs, and may be further extended by structural modifications that minimize degradation.

RNA interference[37] is an endogenous regulatory system of gene expression inhibition, and may be divided in micro RNA (miRNA) and short interfering RNA (siRNA) mechanisms. In RNAi mechanisms, a double stranded RNA molecule is cleaved by Dicer, a class III RNAse. The resulting fragments, about 20 nucleotides long, are inserted in the RISC-loading complex, forming the pre-RISC[38]. Upon degradation of the sense strand by Argonaute-2 (Ago2), the catalytic component of the complex, the RNA-induced silencing complex (RISC) is complete. RISC degrades target mRNA complementary to the antisense strand, and as the structure remains theoretically intact at the end of the reaction, multiple catalytic cycles are possible. siRNA and miRNA differ in the complementary sequence specificity required for target RNA degradation – while siRNA is highly specific, and only regulates transcripts levels that undergo Watson-Crick base pairing on all of the sequence length, miRNA is more promiscuous, as it targets sequences that pair with a short “seed” sequence. So, the latter is involved in the regulation of a much broader set of transcripts and its manipulation for therapeutic purposes is more complex. siRNA has drawn

attention to the potential of antisense degradation of target transcripts, which has high specificity and low toxicity from off-target effects. Nonetheless, off-target effects may arise from RISC incorporation of the antisense strand, and intrinsic regulatory mechanisms may be affected by excessive recruitment of RISC.

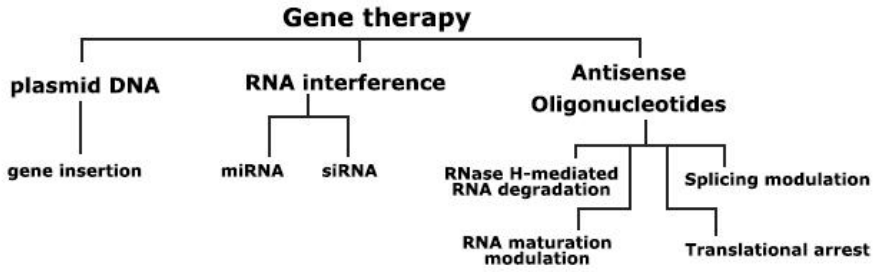

Figure 2 – **Most frequently used gene therapy approaches.**

In a similar mechanism, single stranded **antisense oligonucleotides (AON)** associate with RNAse H to promote degradation of target mRNA, with the possibility of a recycling mechanism and long-lasting effects. Oligonucleotides are designed to have complementary sequences to the target mRNA, which supports high specificity. That may be done with the aid of *in silico* techniques, which take into consideration secondary structures from mRNA folding and protein occupancy that often reduce the available binding regions[39], nevertheless experimental validation is still. Compared to siRNA, AON are not as effective, but as they are easier to manipulate (as seen further below), they have been subject to intensive study for either research or clinical applications. Also, the difference in activity has been tackled by AON structural modifications (explored below). In contrast to siRNA, AON can also work through a number of other mechanisms, namely splicing modulation, RNA processing inhibition, translational arrest, miRNA antagonism and telomerase inhibition.

RNAse H shares with Ago2 a common catalytic mechanism, *i.e.* cleavage of the sense strand from a DNA-RNA heteroduplexes complex, formed between target mRNA and oligonucleotide, and a homolog domain, the catalytic P-element wimpy testis (PIWI) domain[40, 41]. RNAse H is a highly conserved endonuclease, being RNAse H1 is the major isoform in humans, while RNAse H2 is less abundant and requires binding of two proteins (RNAse H2B and RNAse H2C) for activation. The latter is believed to have a role different from RNA degradation, due to its capacity of recognizing and cleaving a single ribonucleotide in a deoxyrribonucleotide strand, *e.g.* a

result of a faulty incorporation during DNA synthesis. RNAse H1, usually referred simply as RNAse H (since RNAse H2 has little importance in the context of AON), was discovered to be influenced by the GC content of the nucleic acid drug. AON with 11 or more guanine or cytosine residues have high efficiency, whereas those with 9 or fewer displayed poor inhibition[42]. Recognition is done by the RNA binding domain (RBD), while cleavage is attributed to the catalytic domain, separated from the former by a spacer sequence. This leads to a shift between the sites where the duplex is recognized and where it is cleaved, of about 7 nucleotide residues (fig. 3)[43]. As cleavage may be hampered by nucleotide structural modifications, gapmer strategies are often employed, as explored later on.

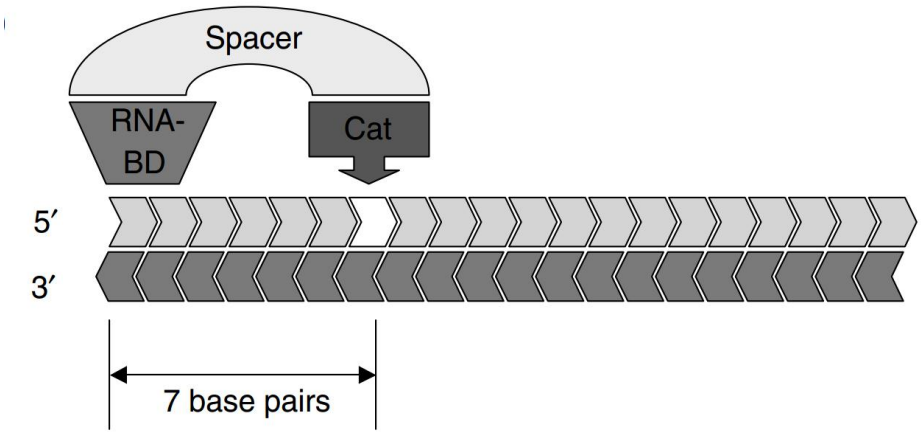

Figure 3 – **RNase H cleavage mechanism.** RNase H cleaves the target strand of a RNA/DNA heteroduplex 7 nucleotide residues away from the recognized sequence[43].

RNAse H is a well characterized and ubiquitous enzyme in mammalian cells, and has been extensively used in antisense therapy, to the point of the number of clinical trials using this mechanism having exceeded the combined number of the antisense oligonucleotides trials that use other mechanisms[43]. This approach benefits from the AON ability to activate RNAse H at low concentrations and rapidly deplete theoretically any target mRNA[39, 43, 44]. Also, it is present in the nucleus, cytoplasm and mitochondria, virtually sustaining AON activity in any intracellular site. However, RNAse H mediated antisense therapies have not yet been used for nerve regeneration[38].

Among other antisense oligonucleotide mechanisms of activity (fig. 4), there is **splicing modulation**, which involves masking splice sequences by AON binding, thus redirecting the pre-mRNA splicing reaction with the production of an altered protein phenotypic profile. Such alterations may have relevant effects, *e.g.* the expression regulation of transcript variants Bcl-X_L and Bcl-X_S regulates apoptosis[45, 46]. **Exon skipping**, a variant of the splicing modulation approach,

has shown to be a valuable tool for correcting specific pathologies such as Duchenne Muscular Dystrophy, which result from different mutations with the ability to disrupt the reading frame[47-51]. AON **inhibition of 3'-polyadenylation** or **5'-capping** may also be used to target mRNA, as it leads to immature molecules, which are subsequently degraded, since this is a crucial step for functional and stability purposes[52].

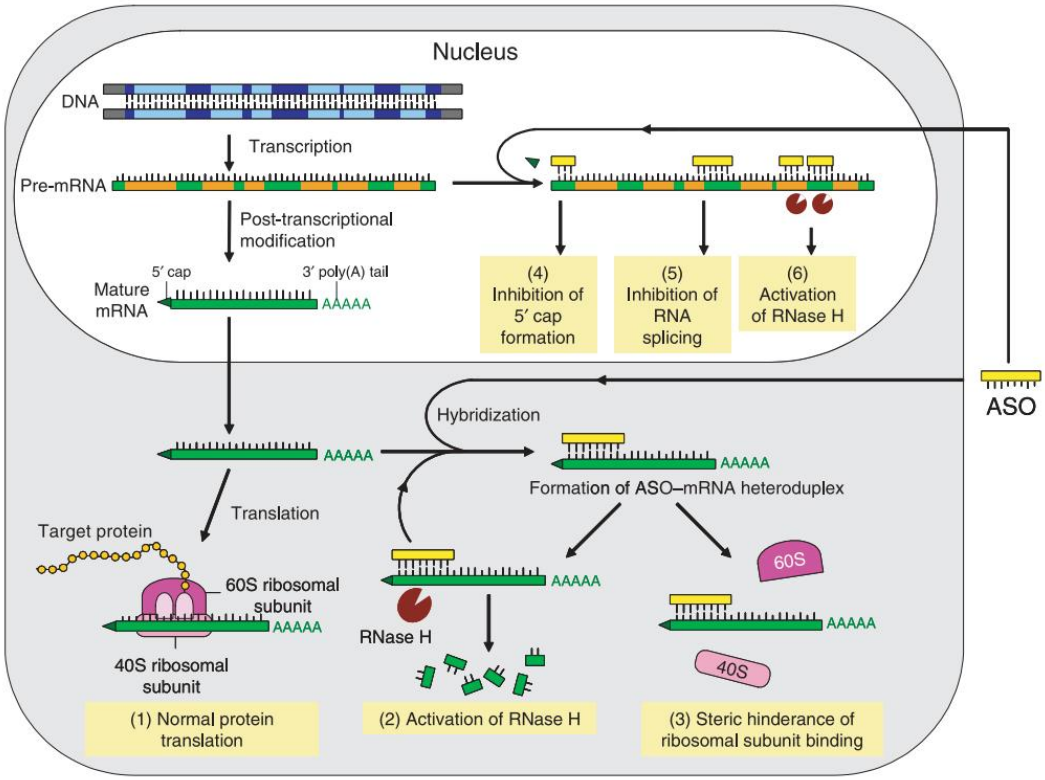

Figure 4 – **Antisense mechanisms[42].** Not only are antisense oligonucleotides able to activate RNase H, they may also interfere with RNA processing and translation mechanisms, lowering protein expression levels all the same. Antisense oligonucleotides may be referred as AON, but also as ASO.

Besides targeting mRNA levels, AON may also be used to inhibit protein synthesis, by a mechanism known as **translational arrest**. It is achieved by AON binding to translational initiation or adjacent regions, thus blocking scanning of the transcript by the 40S ribosome subunit, assembly of the 40S and 60S subunits, or movement of the ribosome down the transcript after assembly. It has been shown to lead to protein downregulation *in vitro*, but confirmation of *in vivo* effects is supported by limited evidence[38]. Since there is no shift in mRNA levels, quantification faces technical issues. miRNA may also be targeted by **miRNA antagonists** that bind and prevent miRNA of participating in RNAi regulation pathways. Although both *in vitro* and *in vivo* experiments

showed promising results, the mechanism is not clearly characterized yet. miRNA degradation is hypothesized, but on the other hand, hybridization with ASO hinders its detection and quantification. Telomerase is a ribonucleoprotein that ensures sufficient telomere length in dividing, *e.g.* cancer, cells. The RNA segment used for binding to telomeres is apt to be targeted by ASO and thus preventing elongation. **Telomerase targeting** has shown promising results for cancer therapy in several studies[53-55].

Although AON are not as efficient as siRNA, structural modifications have been developed to minimize and possibly invert that difference (fig. 5). Pharmacokinetic properties have also been greatly improved due to AON resisting nuclease degradation and evading unspecific interactions that enhance clearance and toxic side effects from off-target delivery[56]. AON modifications are arranged into generations, a classification that relates to their efficiency, extension of modification and relative appearance date. The **first** includes phosphorotioate (PS), a single atom (oxygen to sulfur) substitution on one of the non-bridging atoms of the phosphate group[57]. It improves resistance to nucleases 100-300 fold by a chirality-dependent mechanism (Sp phosphorotioate is nuclease resistant, but Rp is as sensitive as phosphodiester bonds[58]) and increases binding to plasma proteins, which reduces clearance. Thus, circulation time is prolonged and target cells are more easily reached. Neither RNA binding nor RNAse H-activating properties are compromised by this modification[59].

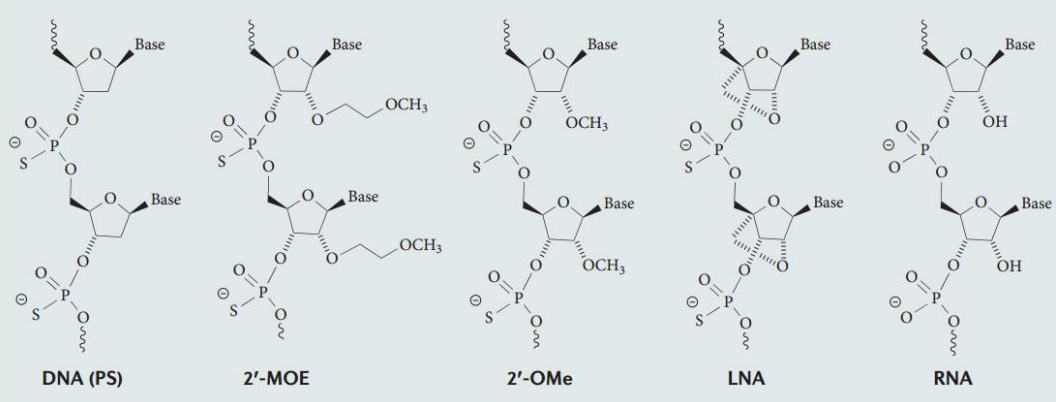

Figure 5 – **AON structural modifications[47].** Newer and more extensive structural modifications (*e.g.* Locked Nucleic Acids) are more effective in downregulating mRNA levels and resisting degradation, but also involve more complex synthesis.

Second generation AON have substituents at the 2' position of the ribose sugar, usually 2'-O-methoxyethyl or 2'-O-methyl[60]. Potency (*i.e.* binding affinity, assessed by the melting temperature, T_m) and stability are higher, but unfortunately RNAse H activation properties are lost. That, however, may be recovered using a gapmer strategy (fig. 6), *i.e.* a center region of the

sequence that allows RNAse H binding, flanked by 2'-modified bases. These modifications lead to longer-lasting effects which in an *in vivo* systemic administration setting of *c-raf*-1 downregulation in humans[61], support a relatively infrequent dosing, e.g. weekly or biweekly dosing[38].

The **third generation** is characterized by extensive alterations to the ribose ring, e.g. substitution by a furanose (morpholino) or by a peptidic backbone (peptide nucleic acid), or conformation constriction (locked nucleic acid). Peptide nucleic acids (PNA) are an example of AON with successful nuclease (and peptidase) evasion, and great biostability. PNA not only selectively bind to target mRNA, but also have anti-gene effects by hybridizing with double stranded DNA in four possible configurations - triplex, triplex invasion, duplex invasion and double duplex invasion[42]. Locked nucleic acids (LNA) have a conformation restriction derived from the 2'-O, 4'-C methylene bridge in the ribose ring, and a greatly increased hybridization affinity. Morpholino nucleotides have a substituted sugar ring, and a high resistance to degradation. Although third generation AON have high T_m and biostability, RNAse H recruitment characteristics are lost. As with second generation AON, gapmer design may solve that problem.

Figure 6 – **Sequence structure of a gapmer.** Modified nucleotides with improved stability and binding properties are included in the flanks. In the center there are nucleotides that enable RNase H activity.

Fomivirsen, an oligonucleotide drug against cytomegalovirus (CMV) retinitis, is the first and, so far, only clinically approved therapeutic oligonucleotide by FDA, in 1998[42, 47]. However, it was discontinued due to low market demand. Fomivirsen is a 21 nucleotide long phosphoriotioate (first generation) oligodeoxynucleotide, and has excellent pharmacokinetic properties. Despite a rapid diffusion to the retinal epithelium after intraocular injection, systemic distribution is remarkably low[60]. The low necessary dose (330 µg per 50 µL), conjugated with the limited systemic distribution, avoided any potential side effects[47]. Other examples of topical or local application yielded good results regarding tissue distribution, but CNS targeting still requires injection to the cerebrospinal fluid, since oligonucleotide do not cross the blood-brain barrier (BBB).

This successful case of PS modifications encouraged its use on most of the drugs currently on clinical trials. Although it has been reported an increase of non-specific interactions with cell surface and intracellular proteins[38, 42], PS remains one of the most successful AON structural modification[62]. A reduction of production costs has been observed, which promises a commercially competitive alternative in the future to currently used drugs[43].

Vector-aided Delivery

Antisense oligonucleotide-based therapies are often required to target a limited cell population, *e.g.* injured neurons. Furthermore, AON are not easily internalized by most cell types. Hence, systemic administration of naked oligonucleotides is not a valid approach. Conjugation with vectors (fig. 7) enables specific, localized delivery and may further improve resistance to degradation, surpass anatomical obstacles and enhance cell uptake. Due to their incomparable ability to deliver nucleic acids into the cytoplasm, modified viruses were among the first vectors to be experimented with. However, issues concerning toxicity, immune response and safety diverted attention to alternatives[63, 64]. Non-viral vector development has presented some valid options so far, but a better understanding of cell entry mechanisms and tissue distribution would greatly benefit the presentation of new, more efficient and safer vectors.

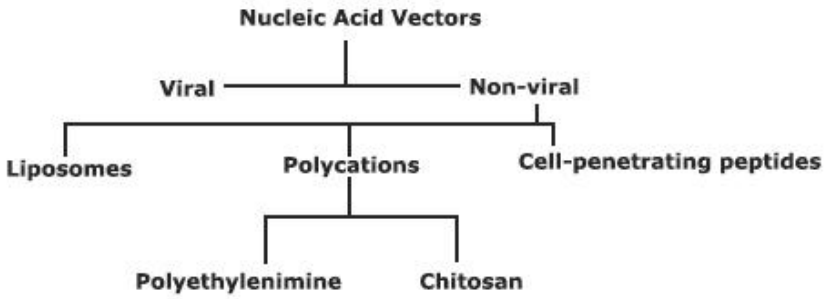

Figure 7 – **Commonly used nucleic acid vectors.**

Non-viral vectors are easier to manipulate and are generally supported by an electrostatic interaction for the formation of complexes with nucleic acids**. Liposome-derived** vectors were among the first vectors studied as an alternative to viral vectors. The cationic lipids in their composition allow the encapsulation of bound DNA in an aqueous inner chamber. A tightly packed structure is formed due to the abundance of electrostatic interactions between the negatively charged phosphate groups of the DNA and the positively vector charged groups. A controlled zeta potential (surface charge) supports interaction with negatively charged membranes and facilitates internalization. As with other vectors, cationic liposomes may be incremented with targeting moieties for a more selective delivery[43]. However, DNA-liposome complexes are associated with several technical obstacles, *e.g.* reducing particle size for a more efficient internalization, toxicity from the cationic lipids, activity decrease in the presence of serum or antibiotics, low encapsulation efficiency, poor storage stability and rapid clearance from the blood, which impair their potential for the delivery of therapeutic nucleic acids in a clinical context[63, 65].

Antennapedia homeodomain and HIV protein Tat were the first described **cell-penetrating peptides** (CPP), resulting from the observation of translocation through biological membranes[66]. The 82 amino acid-long Tat peptide has neurotoxic properties, associated to amino acid residues 31-61, but membrane translocation ability is associated with residues 48-85[67]. Other CPP have been described, usually less than 30 amino acids long, polybasic or amphipatic, and able to carry molecules as they translocate across cell membranes[68]. Cargo molecules are varied, including oligonucleotides that may be covalently or non-covalently bound. The internalization mechanism is not yet characterized, but hypotheses focus on either the endocytic pathway or direct translocation through the plasma membrane, and it may be influenced by cargo size[67], type of CPP[69] and CPP concentration[68]. Endosomal escape mechanisms are not elucidated as well, although suspicions lie on membrane disruption[70].

Although cytotoxicity was not observed in short exposures, long exposures caused extensive cell necrosis[67]. Nonetheless, CPP toxicity is lower than other nucleic acid vectors, since its internalization is fast enough to support short exposures. Transfection efficiency is higher than PEI, the standard vector for nucleic acid delivery. A potential drawback arises from the induction of a humoral immune response against the peptide cargo[67], which may be useful in DNA vaccination approaches[71]. In order to use CPP in a clinical context, several issues should be addressed, namely characterizing mechanisms of internalization, endosomal escape, cargo size influence, as well as affinity and specificity. There is also the matter of production costs, which may be reduced once CPP enter larger-scale applications. Additionally, CPP, as other peptides, have not been used in oral administration so far[68].

Polyethylenimine (PEI) is one of the most studied and promising polymeric vectors. After cellular internalization, its high buffering capacity leads to a rapid endosomal escape by a process referred as proton-sponge effect. As with lipoplexes, PEI polyplexes are victim to extensive aggregation from non-specific interactions with plasma proteins. Blood circulation may be prolonged by polyethylene glycol (PEG) coating, *i.e.* PEGylation, a commonly used protective technique[66, 72]. Cytotoxicity rises with the augment of the proportion between PEI and the nucleic acid drug. Complex size, surface charge and transfection efficiency are also influenced, *i.e.* the charge ratio between the polymer amino groups and the phosphate groups of the nucleic acids (N/P ratio) has a profound influence as a formulation determinant. Efficiency is described as optimal at N/P 8 for plasmid transfection, but it is associated to significant toxicity[73].

Chitosan is a deacetylated derivative from chitin, a β1→4 N-acetylglucosamine anionic polyssacharide and the major component of crustaceans and insects exoskeleton and fungi cell

wall. It is a biocompatible and biodegradable material with low toxicity, high cationic potential and has functional groups that allow simple coupling of extracellular and intracellular targeting ligands[63]. It has been extensively used in gene therapy studies[74-77]. However, before regarding the possibility for its use as a gene carrier in clinical trials, low specificity and low transfection issues must be solved. The latter is highly dependent on formulation, especially on molecular weight (MW), degree of deacetylation (DD), pH (solubility), and charge ratio of chitosan to DNA. High DD ensures vector positive charge by exposing amino groups with a pK_a around 6.5[64, 78]. The electrostatic binding between the positively charged chitosan amines (N) and the negatively charged DNA phosphates (P) is also dependent on the charge ratio, *i.e.* N/P ratio. An adequate ratio must provide complex stability in a physiological milieu, but also enable disassembly after entering the target cell. High ratios grant complex integrity, but may limit drug release and lead to some cytotoxicity. MW influences DNA entrapment, a decisive factor in nuclease evasion, and delivery upon cell entry. These major formulation factors affect each other, *.e.g.* increasing N:P ratio for better stability may be compensated by lowering MW in order to maintain release capacity and high transfection efficiency[79].

pH affects solubility and electrostatic interaction since it may determine whether the amino groups are protonated or not, *i.e.* positive charge is ensured only at acidic pH, but not at physiological conditions[80]. That issue has been addressed with the use of chitosan salts, *e.g.* with chitosan hydrochloride (CHy), chitosan lactate (CLa), chitosan acetate (CAc), chitosan aspartate (CAs), chitosan glutamate (CGl), that increase transfection efficiency, but also raise optimum N:P ratios[65]. The use of **trimethylated chitosan** (TMC) is another solution, since it sustains a constant positive protonated state on the amino groups by covalently binding three methyl substituents. TMC supports higher solubility and DNA binding, and also increases the complex zeta potential, which enhances interactions with the negatively charged cell membranes. An increase in membrane permeability for small hydrophilic compounds has also been observed, nonetheless maintaining a level of cytotoxicity lower than PEI[81].

Additional structural modifications may also be used. Examples include the introduction of the non-toxic fragment of the tetanus toxin for targeting nanoparticles to neuronal cell populations[82], or **hydrophobic moieties** that increase hydrophobic interactions with single stranded AON, cell membranes, and endosomal membranes, which enhance complex formation, internalization and endosomal escape, respectively[83]. There are other strategies, like the use of fibrin scaffolds that enable controled complex release[84], or of double stranded oligonucleotides that are more stable and bind more easily to polycations[85] (due to increased charged density and lack of exposure of hydrophobic bases to the solvent) than single stranded oligonucleotides. Furthermore, endosomal escape may be addressed by chemical modification with lysine-hystidine dendrons that improve

buffering properties and stimulate the proton sponge effect[83, 86]. All in all, there are several approaches for increasing the efficiency of polycation-mediated nucleic acid delivery.

This project was part of a study aimed to develop an approach for the induction of nerve regeneration after SCI by downregulating RhoA and GSK3β. A battery of antisense oligonucleotide sequences were designed and tested for their capacity to down-regulate the target molecules. Based on the results they are expected to be later further developed into more efficient oligos by introduction of 3rd generation nucleotide modifications. A newly developed nucleic-acid delivery platform consisting of trimethylated chitosan conjugated with a hydrophobic group was assessed for the capacity to deliver antisense oligonucleotides *in vitro*. If successful, this would warrant further development of the platform for future *in vivo* delivery targeting neuronal cells in the context of SCI nerve regeneration.

Methods

AON design

AON sequences (table 1 and 2) were previously determined based on binding properties (optimized Tm) to available sections of the target mRNA taking into consideration RNA secondary structure (using the web-based software "oligo analyzer" from IDT and "SFold"[87]). Other putative targets were not found using a BLASTN screening for unspecific binding. 22 nucleotides-long gapmers were produced and purified by GE Health Care Uppsala, Sweden, in which the 10 central nucleotides were phosphorothioate-modified and the six nucleotides in each end were phosphorothioate- and 2'-O-methyl-modified, as seen on tables 1 and 2. This gapmer structure is believed to sustain RNase H activity. The 7th sequence of both the RhoA and the GSK3β AON sets differs in structure by having no phosphoriothioate bonds between the 2-O-methyl substituted nucleotides; that change was done in order to assess the potential redundancy of having both structural modifications in the same segment. These sequences were designed for rat gene targeting, since testing has been planned to proceed in murine animal models; they may be substituted by other sequences if another species is to be targeted.

Table 1 – **RhoA AON sequences.** "*" refers to a phosphorothioate bond, that substitutes the typical phosphodiester one, and nucleotides preceded by "m" have 2-O'-methyl modifications. RhoA AON 6b has a similar nucleotide sequence to RhoA AON 6 but differs from all other AON by not having phosphorothioate bonds between the 2-O-methyl-substituted nucleotides.

RhoA AON 1	mU*mA*mC*mC*mU*mG*C*T*T*C*C*C*G*T*C*C*mA*mC*mU*mU*mC*mA
RhoA AON 2	mA*mU*mC*mU*mU*mC*C*T*G*T*C*C*A*G*C*T*mG*mU*mG*mU*mC*mC
RhoA AON 3	mC*mU*mC*mC*mC*mG*C*C*T*T*G*T*G*T*G*C*mU*mC*mA*mU*mC*mA
RhoA AON 4	mA*mC*mC*mU*mC*mU*C*T*C*A*C*T*C*C*G*T*mC*mU*mU*mU*mG*mG
RhoA AON 5	mC*mC*mG*mA*mC*mU*T*T*T*T*C*T*T*C*C*C*mG*mC*mG*mU*mC*mU
RhoA AON 6	mA*mU*mC*mU*mC*mU*G*C*C*T*T*C*T*T*C*A*mG*mG*mU*mU*mU*mU
RhoA AON 6b	mAmUmCmUmCmUG*C*C*T*T*C*T*T*C*A*mGmGmUmUmUmU

Table 2 – **GSK3β AON sequences.** "*" refers to a phosphorothioate bond, that substitutes the typical phosphodiester one, and nucleotides preceded by "m" have 2-O'-methyl modifications. GSK3β AON 6b has a similar nucleotide sequence to GSK3β AON 6 but differs from all other AON by not having phosphorothioate bonds between the 2-O-methyl-substituted nucleotides.

GSK3b AON 1	mA*mA*mA*mG*mG*mA*G*G*T*G*G*T*T*C*T*C*mG*mG*mU*mC*mG*mC
GSK3b AON 2	mC*mC*mU*mC*mA*mU*C*T*T*T*C*T*T*C*T*C*mG*mC*mC*mA*mC*mU
GSK3b AON 3	mG*mG*mU*mU*mC*mU*G*T*G*G*T*T*T*A*A*T*mG*mU*mC*mU*mC*mG
GSK3b AON 4	mC*mA*mG*mU*mU*mC*T*T*G*A*G*T*G*G*T*A*mA*mA*mG*mU*mU*mG
GSK3b AON 5	mG*mA*mG*mG*mA*mG*G*G*A*T*A*A*G*G*A*T*mG*mG*mU*mG*mG*mC
GSK3b AON 6	mU*mU*mC*mU*mC*mA*T*G*A*T*C*T*G*G*A*G*mC*mU*mC*mU*mC*mG
GSK3b AON 6b	mUmUmCmUmCmAT*G*A*T*C*T*G*G*A*G*mCmUmCmUmCmG

Cell Culture

The adherent RN22 (Rat schwanomma), and HeLa/Luc705 (Human cervical adenocarcinoma) cell lines were used. The latter expressed non-functional Luciferase due to a mutated intron; this cell line is used as reporter system for efficient transfection of a specific, splice-correction AON, since it can trigger RNA expression of functional Luciferase, quantifiable by a functional assay[88]. The cells were cultured at 37ºC, 5% CO_2, in T75 culture flasks (Thermo Scientific) in approximately 10 mL of Dulbecco's Modified Eagle Medium (DMEM) supplemented with 10% fetal bovine serum (FBS) and 50 µg/mL gentamicin, henceforth referred as "complete medium". Subcultures were done routinely to prevent overconfluency, by washing the cells with 5 mL of phosphate buffer saline (PBS) and addition of 1 mL 0.25% (w/v) trypsin. Cells were then suspended in an appropriate volume of complete medium, thus inactivating trypsin, and re-seeded at the desired cellular density.

Cellular transfection

500 µL of cell suspension was used for seeding 24-well plates (BD Falcon) at adequate density so that 50-60% confluency was reached after 24h, *i.e.* at the moment of transfection, and overconfluency was not reached before the experiment ended. GSK3β and RhoA AON were transfected with TransIT-Oligo (Mirus). Although AON and transfection reagent concentrations varied, the transfections were done by adding 50 µL of the transfection mix, containing Opti-MEM I Reduced Serum Medium (Invitrogen), Transit, and the AON, to 250 uL medium. TMC transfections were done by adding 50 µL of the prepared complex solution to 450 µL medium. In both cases, the medium was substituted immediately before the transfection for antibiotic-free medium, and was only re-added 4h after. Chloroquine at 100 µM (final concentration) was added to selected samples at 24h after transfection; medium was replaced by complete medium 4h later.

RhoA- and GSK3β-AON sequence screening

Total RNA of RN22 was harvested at 24h after transfection with TransIT-Oligo, with the Direct-zol RNA MiniPrep kit (Zymo Research). NanoDrop 1000 (Thermo Scientific) spectrophotometric analysis was used for determining RNA concentration of the extracts and accessing purity levels by the 260/280 ratio (should be equal or higher than 2). Equal amounts of total RNA were amplified by OneStep RT-PCR kit (Qiagen), or by SuperScript II reverse transcriptase (Invitrogen) followed by HotStar Taq DNA polymerase (Qiagen). A minimum of 3

independent replicates were done for each condition.

Every sample was submitted to amplification of both the target (GSK3β or RhoA) and a reference (rRNA) gene. 15 µL PCR products with 3 µL loading buffer were submitted to 1.2% agarose gel electrophoresis at 100V for 70 minutes and semi-quantitative analyzes performed using the Volume tool of the Image Lab (Bio Rad) software for band intensity. Relative transcript levels are defined by dividing the ratio of target to reference gene of each sample by the equivalent ratio of the untreated, negative control sample.

Complex formation

The biomaterials under study were previously prepared and characterized in the lab. The unmodified TMC had 43.3 kDa, 11% acetylated monomers and 30% quaternized monomers. The modified materials had similar characteristics with an additional degree of stearic acid substitution which is indicated below. All TMC solutions were done in 10 mM HEPES and 5% (w/v) glucose, in the pH range of 7.2-7.4, as determined by an 827 pH Lab Meter (Metrohm).

TMC-AON or SA TMC-AON complexes were prepared immediately before any experiment, following a common protocol with a usually fixed oligonucleotide concentration at 1 µM and a variable concentration of TMC. The AON used in the TMC analyses was 20 nucleotides long with phosphoriothioate modifications (C*C*U*C*U*U*A*C*C*U*C*A*G*U*U*A*C*A), in other words, similar to the AON under screening for downregulation activity.

The complexes were prepared by separately heating the AON and TMC solutions at 60ºC for 5 minutes, then adding the AON solution to the TMC solution, and heating the mixture at the same temperature (60ºC) for 15 minutes under agitation, followed by a cooling down period at room temperature (approximately 25ºC) for 30 minutes. Some samples, *i.e.* those submitted to gel retention, DLS, TEM and nucleic acid binding dye accessibility analyzes, were also further incubated in PBS for 30 minutes at room temperature (approximately 25ºC), which aimed to simulate physiologic salt and pH conditions.

Complex characterization

Gel retention electrophoresis assay

The prepared complexes were analyzed for the TMC binding properties, by gel retention

electrophoresis assay. For agarose gels, 2% agarose (w/v) was dissolved in TAE buffer (Tris base, acetic acid and EDTA), added SybrGold for antisense oligonucleotide staining using the recommendations of the manufacturer, and run under 120V for 30 minutes. Samples contained 25 µL complexes, 2 µL MilliQ water, 3µL 10x PBS and 6 µL loading buffer. Gradient polyacrylamide gels (4-20%) were also used and ran at 80V for 45 minutes. PAGE gels were stained after the run by incubation in 1x SybrGold in TBE solution for 15 minutes. Gel imaging was done using a ChemiDoc (Bio Rad) camera equipment.

Nucleic acid binding dye accessibility assay

The samples, previously incubated in PBS, were further incubated with 1x SybrGold for 10 minutes at room temperature (approximately 25ºC). Fluorescence emission was determined by exciting the samples at 495 nm and detecting at 540 nm. Blank solutions were prepared with the same TMC concentrations as the samples, but with no AON, and a free oligonucleotide sample was also prepared, with no TMC. Three independent replicates were prepared for each condition, each analyzed in duplicate.

Dynamic Light Scattering analysis

Dynamic Light Scattering (DLS) analysis was done using a Zetasizer Nano (Malvern), with three independent replicates observed three times each. Between each separate analysis, the cuvette was washed with MilliQ water.

Transmission Electron Microscopy

Transmission Electron Microscopy (TEM) analysis was prepared by placing the samples over a formvar-coated carbon grid, dehydrating them and performing negative staining with 1% uranyl acetate.

Transfection studies

Luciferase assay

An additional method was used for assessing the transfection efficiency, a reporter system in which the used HeLa cell line expresses a non-functional Luciferase gene. Upon efficient transfection of a specific AON, the induction of a splice-correction mechanism leads to the

expression of functional Luciferase. In order to evaluate relative Luciferase expression levels, cells were washed with 500 µL PBS, lysed with 300 µL HEPES-Krebs-Ringer solution (containing 10mM glucose, 1.2 mM $CaCl_2$, 5 mM KCl, 1.2 mM $MgSO_4$, 1.2 $NaHPO_4$, 130 mM NaCl and 0.15% Tryton X100), stored at -80 ºC for 10 minutes, and then left to thaw at room temperature (approximately 25 ºC) for about 30 minutes. Then, the cell lysates were analyzed with both the Luciferase Assay System Kit (Promega) and the Micro BCA Protein Assay Kit (Thermo Scientific). The former determines luciferase levels through emitted luminescence and the latter determines total protein levels through absorvance at 562 nm. Relative luciferase levels were calculated by establishing the ratio of luciferase to total protein levels, and then the fold increase between the samples and the non treated control.

Flow cytometry

Transfected cells were analyzed in a FACS Calibur (BD), 24h after transfection. The used AON were labeled with Cy5. Cells were suspended by trypsin treatment, washed with 500 µL cold PBS, and filtered through a 100 µm pore filter before the analysis.

Fluorescence microscopy

Samples were visualized at 24h after transfection with an AxioVert Inverted Fluorescence Microscope (Carl Zeiss).

Results

PART I – Nucleic acid drug

Selection of transfection conditions

During optimization of the transfection conditions, an approach with fluorescence chromophore (Cy5)-labeled antisense oligonucleotides was used. The optimum conditions were selected for antisense activity screening of oligonucleotide sequences with a commercial reagent specific for *in vitro* transfection of these nucleic acids, TransIT-Oligo (Mirus). Gentamycin was removed from the cell culture medium during the initial 4h of transfection, since it is reported that the presence of antibiotics during transfection may lead to substantial cytotoxicity[59]. Flow cytometry was used as an initial approach to assess AON association/internalization to cells. This technique does not entirely differentiate between membrane-bound or internalized AON; furthermore, those that enter the cell may be either contained in endocytic vesicles or free in the cytoplasm and nucleus, where they are able to exert their function. In other words, conclusions on transfection efficiency may not be gathered solely from flow cytometry analysis, however a higher degree of relative fluorescence normally relates to increased possibilities of achieving higher transfection efficiency. It is thus useful for a simple and quick screening, which is complemented later by functionality studies.

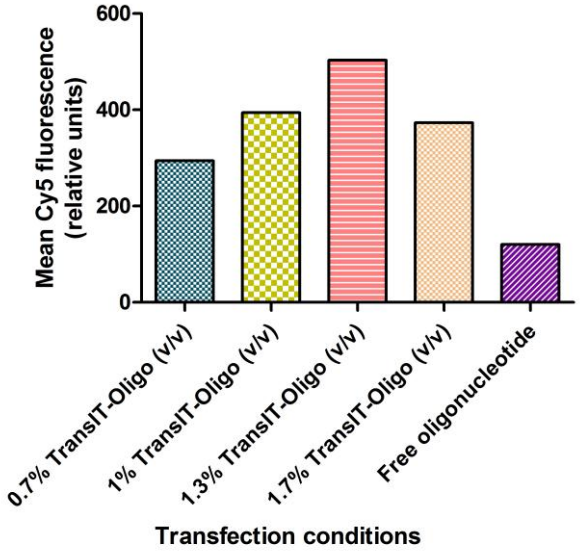

Figure 8 – **Mean fluorescence of flow cytometry studies at 0.1µM AON.** Several concentrations of TransIT-Oligo (Mirus), a commercial transfection reagent were tested, alongside a free oligo control.

From the analysis of the mean fluorescence of each sample, 1.3% TransIT-Oligo (v/v) can be expected to support efficient AON transfection in the selected cell line (RN22) since it supported the highest fluorescence levels (fig. 8). Some cytotoxicity (verified by observation of cell morphology under the optical microscope) was seen for the sample with the highest transfection reagent concentration, which may explain the difference of fluorescence to the previous sample. At 0.1 µM, fluorescence level is increased more than 3 times by the presence of 1.3% transit; however, as stated before, no straight-lined conclusions may be gathered from flow cytometry analysis alone.

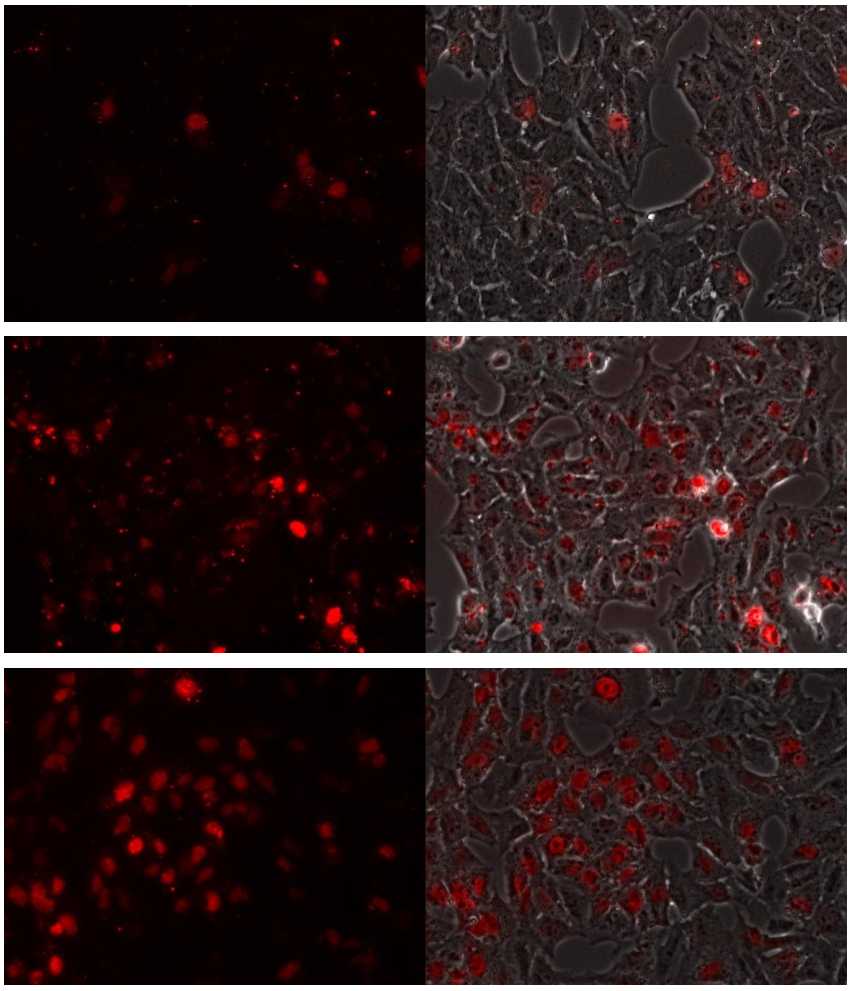

Figure 9 – **Fluoresnce microscopy analysis of different transfection reagent concentrations.** Free oligo at 0.1 µM (top), 1.3% (v/v) TransIT-Oligo and 0.1 µM AON (middle) and 1.3% (v/v) TransIT-Oligo and 0.3 µM AON (bottom). The pictures were taken at 40x zoom, and at identical exposures times.

Following the flow cytometry studies, fluorescence microscopy was used to confirm whether the previously selected conditions were efficient in transfecting the selected cell line. In addition to free oligo and 1.3% (v/v) TransIT-Oligo at 0.1 uM AON, 1.3% (v/v) TransIT-Oligo at 0.3 µM AON was also tested, having had their microscopy pictures taken at identical exposure times. The latter provided substantially higher transfection efficiency with no significant signs of cytotoxicity (fig. 9). Efficient transfection was determined by diffuse nuclear staining, referred in previous studies as a characteristic of phosphorothioate-modified AON[89, 90]. In opposition, cytoplasmatic abundance of small granules is signal of extensive retention of AON at vesicles, most probably endosomes, *i.e.* there is low endosomal escape.

A manual counting of nuclear- or cytoplasmic/vesicular-stained cells was done from fluorescence microscopy images, and used in a contingency table (table 3). For analysis purposes, cells binned into the first class were excluded of the second, although in reality they are stained in the cytoplasm as well. The chi-square test returned $p < 0.001$ that the data is statistically significant, *i.e.* the statistical analysis supports that the tested conditions have different transfection properties.

Table 3 – **Contingency table used in the analysis of the fluorescence images**. Cell count was determined manually. P<0.001 statistical significance analysed by chi-square test of the 2x3 contingency table.

	Nuclear localization	Cytoplasmatic/vesicular localization/Unstained
Free ON 0,1 uM	10	88
TransIT 1,3% 0,1 uM	22	56
TransIT 1,3% 0,3 uM	19	81

Since these results from the optimization studies support 1.3% (v/v) TransIT-Oligo and 0.3 µM AON as efficient transfection conditions with about 80% transfected cells, these were selected for further testing of AON downregulation activity.

Analysis of antisense oligonucleotide activity

Rn22 a rat schwannoma cell line expressing RhoA and GSK3beta was then used as a model for testing the downregulation efficiency of a series of antisense oligonucleotides. These were selected previously based on thermodynamic analysis of binding affinities of the oligos to the target mRNAs (having in consideration melting temperatures and RNA secondary structure). After transfection with conditions determined from the results presented above, reverse transcription PCR with semi-quantitative analysis was selected as an initial method to screen for the different oligonucleotide efficiencies.

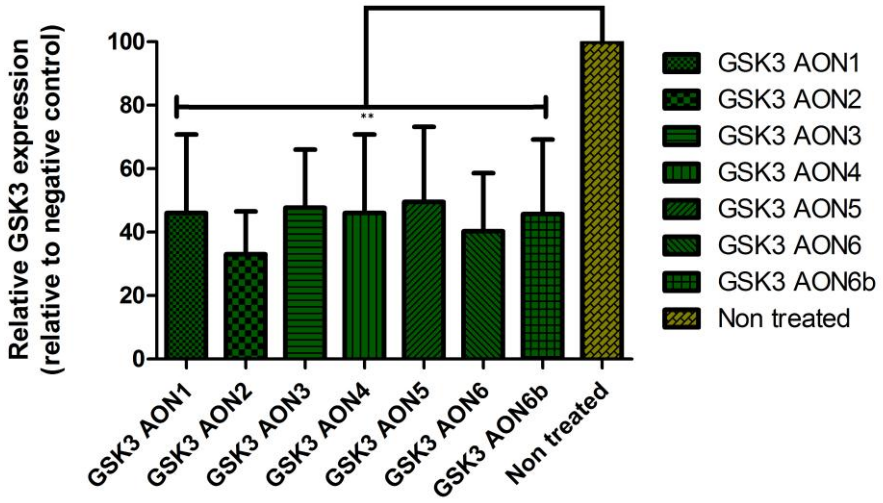

Figure 10 – **Antisense activity analysis of GSK3 AON-treated, PCR-amplified samples.** There is a clear downregulation of the target gene (**p < 0.01, samples vs non-treated), although high variability hinders an effective comparison between the different sequences (not statistically significant).

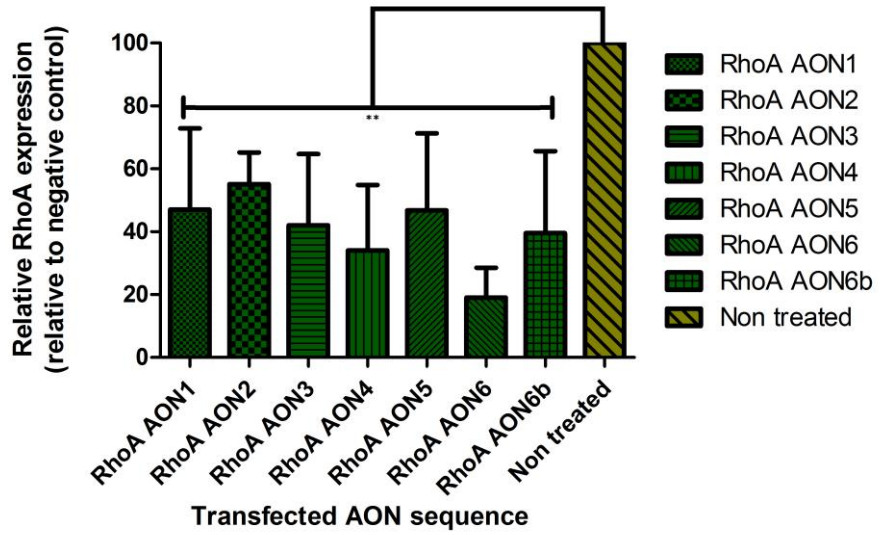

Figure 11 **- Antisense activity analysis of RhoA-AON treated, PCR-amplified samples.** There is a clear downregulation of the target gene (**p < 0.01; samples vs non-treated), although high variability hinders an effective comparison between the different sequences (not statistically significant).

This semi-quantitative means of analysis yielded a very high standard deviation, which did not enable sequence discrimination (fig. 10 and 11). Nonetheless, all of them were effective in downregulating the target gene. The variability observed in the antisense studies could reflect some toxicity issues observed during the transfection procedure with some of the AONs (as seen by cell morphology changes visualized under the light microscope – data not shown). Despite the variability and the absence of statistical significance between every pair of treated samples, all AON sequences tested yielded gene downregulation with $p < 0.01$. Based on these results quantitative, real-time RT-PCR will be used in future to confirm and better discriminate between some of the AON sequences.

PART II – Polymer vector

In order for antisense oligonucleotides to have effects in a therapeutic context, they need to be delivered to target cells in an efficient way. Due to their chemical nature (negatively charged hydrophilic molecule), these are not taken up efficiently by cells; furthermore, pharmacokinetics and bioavailability are an issue in *in vivo* conditions. Thus, safe and non-toxic delivery vectors are needed for therapeutic applications of antisense oligonucleotides. In that context, chitosan, a natural polymer with inherent biodegradability properties, is a promising vector.

A new chitosan derivative was tested for efficient complexation (formation of nanoparticles) and for transfection efficiency of AONs. Trimethyl modification of the deacetylated amines of chitosan produced a biomaterial with improved electrostatic interaction and solubility properties, trimethylchitosan (TMC). An additional modification with stearic acid was tested for AON binding properties, nanoparticle diameter, cellular binding and transfection efficiency properties, which were expected to improve over the unmodified TMC.

Physical and chemical properties of TMC

Unmodified TMC and stearic acid conjugated TMC (TMC-SA) were tested for the ability to bind to AONs. Initially, a TMC-SA with 5% SA (TMC-SA 5%) modification was tested. Later in the project a TMC-SA with 2.5% SA (TMC-SA 2.5%) modification became available, which was included in some of the analyses. An initial approach to study the AON binding properties of both the unmodified and TMC-SA 5% was done by using agarose gel electrophoresis and SybrGold staining. Since the nucleic acid dye should only bind free oligonucleotides, this was perceived as a simple and effective analysis. Using a free oligo control as a reference for migration length, several TMC N/P ratios could be tested for their ability to strongly interact and bind AON thereby preventing its migration in the gel. AON weakly interacting or not interacting at all with the TMCs after complexation will migrate. The fraction of migrating AON thus directly reflects the extension of interaction between AON and TMCs.

The smearing pattern observed is indication that the oligonucleotide is also being released from the interaction with the TMC over time (during the agarose run). This could indicate a destabilizing effect of the nucleic acid binding dye (SybrGOLD which was present in the gel during the electrophoresis) and/or the electrophoresis voltage conditions. Presence of a smear but absence of free oligo band suggests complete AON binding at the beginning of the run, with posterior release during the run.

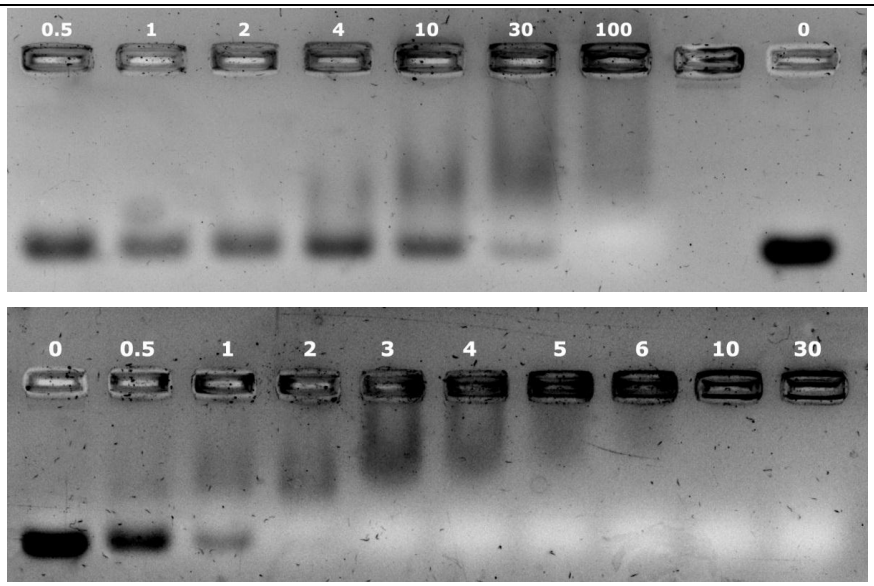

Figure 12 – **Agarose gel retention assay of unmodified TMC (top) and 5% stearic acid-substituted TMC (bottom).** N/P ratios are indicated above each column, 0 indicates free oligo (no TMC present). The unmodified TMC has much weaker AON binding properties than the stearic acid-modified TMC. The former has partial retention at N/P 30 and complete retention at N/P 100, while the latter has partial retention at N/P 1 and complete retention at N/P 2.

As expected, the hydrophobic substitution was effective in improving the AON binding properties of TMC, since at N/P 2 no free oligo was present at the beginning of the run (fig. 12); however, the intense smear indicates potential low interaction stability. Higher N/P ratios have reduced smear, and at N/P 10 and 30, there is none at all. Although it lacks confirmation in vitro, excessive N/P ratios may pose an obstacle to oligonucleotide release after entering the cell, in the case of the interaction being too stable and the complex failing to dissociate. Cytotoxicity could be another valid reason to avoid those N/P ratios. Although the hydrophobically modified TMC (with 5% SA modification) showed complete retention of the oligo at low N/P ratios, the unmodified trymethylchitosan was only effective in slowing the AON migration at N/P 100 (although some degree of destabilization is still observed – presence of smear).

A different approach was used at a later stage – considering that the presence of nucleic acid binding dyes during the electrophoresis could interfere with AON migration, posterior staining was suggested. Polyacrylamide gels were selected because they are more efficient in post staining than agarose gels. For this analysis, unmodified TMC, TMC-SA 5% and TMC-SA 2.5% were available to use.

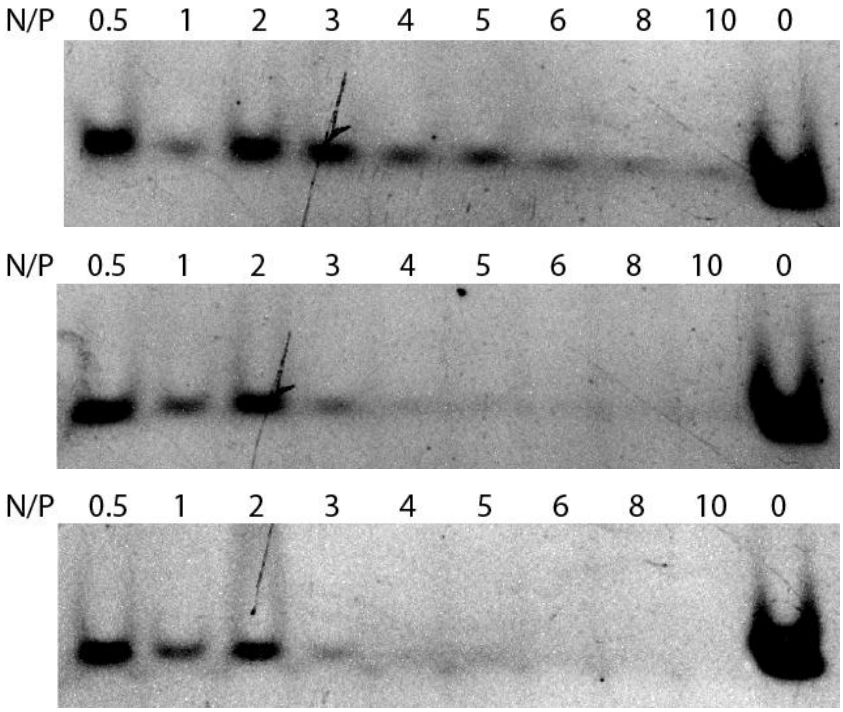

Figure 13 – **Polyacrylamide gel retention assay of unmodified (top), 2.5% stearic acid-modified (mid) and 5% stearic acid modified (bottom) TMC.** Polyacrylamide gels enable nucleic acid staining after having been run, contrary to agarose ones. The difference in the results supports that SybrGold has a destabilizing effect on TMC-AON interaction, especially on unmodified TMC samples. In other words, stearic acid-modified TMC produces more robust interactions with AON.

The difference between both sets of results indicates that there was an influence of the nucleic acid dye presence during the electrophoresis on the interaction stability and oligonucleotide migration. SybrGold appears to have a destabilizing effect during the run, possibly by competing with TMC for AON binding. The smear is not present in the polyacrylamide gels, probably because the complexes were not destabilized in the absence of SybrGold during the electrophoresis analysis, thus not releasing oligonucleotide.

This destabilizing/competing effect of a nucleic acid binding dye has not been reported previously in the literature and was initially unexpected. However, these two behaviors made possible to draw extra conclusions. As a competing effect is seen between the cationic polymer and SybrGold for binding to the oligonucleotide, this in principle allow us to directly observe another level of binding strength for the unmodified and SA-modified TMCs. Hence, whereas the destabilizing effect of SybrGold is only seen with TMC-SA 5% up to N/P ratio 5-6, for the unmodified TMC this destabilization is seen up to N/P 100 (notice the smear band). This provides another level of confirmation for the stronger interactions between the TMC-SA and oligonucleotide, especially when in presence of a destabilizing condition.

In polyacrylamide gels, the difference in band intensity between the TMC-containing samples and the free oligo control is much more obvious (fig. 13) than in agarose gels. The TMC-SA 5%, as well as the TMC-SA 2.5%, shows almost complete retention at N/P 3, a value approximate to the one previously obtained – the increase in that result may be related to the higher sensitivity of polyacrylamide over agarose gels. The biggest change is observed in the unmodified TMC, which in the agarose gel retention analysis showed retention only at N/P 100, a very high amount of polymer, whereas in the polyacrylamide gels, retention is almost complete from N/P 5 onwards. The destabilizing effect is clearer in the unmodified TMC samples than in the stearic acid-modified TMC samples, *i.e.* the latter produces a more robust interaction with AON.

Despite the reviewed difference between both methods of analysis, it is clear that the stearic acid hydrophobic moiety introduced in our biomaterial of study, trymethylchitosan, was successful in improving AON binding properties. No major variance was recorded between the materials with different degrees of stearic acid modification.

The same nucleic acid dye used in the gel retention studies was used in a parallel experiment, with a simpler concept. In the SybrGOLD accessibility assay, fluorescence intensity levels of SybrGOLD are dependent on its binding to AON, which in turn is dependent on AON binding properties and nanoparticle structure of TMC. Accessibility to nucleic acid binding dye was considered complete (100%) for the free oligo control sample. PBS incubation was expected to efficiently mimic physiologic pH and salt conditions. The increase in ionic strength may shield charged moieties and interfere with electrostatic interactions, which are crucial for maintaining the complex integrity. This method of analysis determines whether upon complexation with the polymer vectors, AON is accessible to the nucleic acid dye binding. This might be dependent not only on whether the oligonucleotide is TMC-bound but also on structural properties/arrangement of the complexes.

Most of the unmodified TMC N/P ratios yielded fluorescence levels around 50% of those from the free oligo control (fig. 14), which was unexpected, considering that the results from retention studies determined a much lower fraction of unbound AON, especially for the higher N/P ratios. Also, previous studies with similar analyses [65, 91] showed a curve that has residual levels of fluorescence after a N/P ratio associated with complete AON binding. That did not happen here, since there is a marked rise in fluorescence after N/P 2.

Both N/P 1 and 2 have much lower fluorescence levels than the remaining samples. Seeing that the stoichiometry of opposite charged moieties is close to 1:1, it was proposed that mutual

charge neutralization was responsible for the absence of electrostatic repulsion between nanoparticles and consequential aggregation. This is supported by the intrinsic aggregation properties of chitosan and chitosan derivatives[92]. Aggregation is expected to entrap oligonucleotides and prevent their accessibility to nucleic acid dye binding. Validation of this hypothesis requires further analyses.

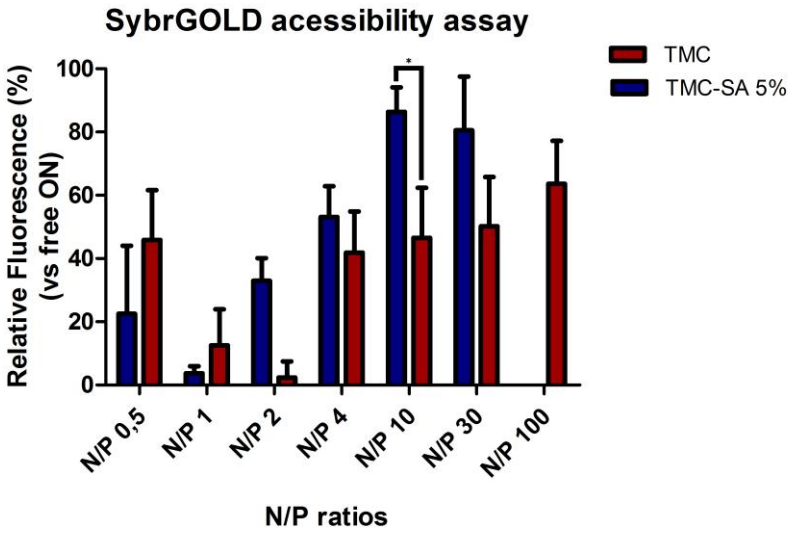

Figure 14 – **Relative fluorescence levels, in comparison to the free oligonucleotide control, of the SybrGold analysis of unmodified TMC and TMC-SA 5%.** N/P 100 of TMC-SA 5% was not tested. Most values are higher than expected, given the results from retention studies. A loose, disorganized structure is a viable hypothesis for the reduction of SybrGold exclusion from nucleic acid dye binding. The low fluorescence values at TMC N/P 1 and 2 and TMC-SA 5% N/P 1 may be due to extensive aggregation, from mutual neutralization of opposite charges. The hydrophobic properties of the stearic acid substituents support the formation of an uncompacted micelle-like particle structure of TMC-SA 5%-AON complexes that allows accessibility of TMC-bound AON to SybrGold binding. TMC N/P 10 is statistically significant from TMC-SA 5%, *p<0.05.

Similar to the unmodified TMC, the stearic acid-modified fluorescence levels were higher than expected, especially for higher N/P ratios. At N/P 1, the event of nanoparticle (NP) aggregation proposed for N/P 1 and 2 of unmodified TMC is likely to have been repeated. N/P 0.5 has a high standard deviation, as some instability is associated to this condition. Both TMCs show a tendency for increased association of SybrGOLD to nucleic acid with increasing N/P ratios although TMC-SA5% seems to reach a plateau at N/P10 while unmodified TMC, shows a tendency for lower fluorescence levels ($P<0.05$ for N/P10).

This effect could be possibly explained due to formation of a loose, disorganized particle structure that enables access of a nucleic acid binding dye to TMC-bound AON. The slight intrinsic hydrophobicity of TMC[81] supports that hypothesis. Thus, this analysis was called accessibility

assay instead of the common designation of nucleic acid binding dye exclusion assay. The emitted fluorescence is specific for SybrGold-AON binding since solutions with only TMC, and no AON were prepared alongside the samples under test to correct for background levels of fluorescence due to the presence of the polymer (thus eliminating unspecific fluorescence).

The higher fluorescence levels (high binding of SybrGOLD to nucleic acids) of TMC-SA5% could be attributed to the introduction of hydrophobic moieties with increasing N/P ratios apparently stimulating this phenomenon. This could possibly be related to the formation of a micelle-like structure, in which the acyl chains are preferably located at the NP core, and the TMC backbone is found at the NP surface[93]. The latter supports the high AON accessibility to nucleic acid dye binding since the former have a higher tendency to bind to the quaternary amines of the TMC backbone, and these could be preferentially located at the surface, *i.e.* they are highly exposed to the polar solvent.

Average particle diameter were determined by Dynamic Light Scattering analysis, both for N/P 5, where interaction of AON with TMC and SA-modified TMC was almost complete or complete, respectively, and N/P 80 which was the highest ratio reached with each biomaterial under study (unmodified, 2.5% SA and 5% SA TMC), after incubation in PBS. PBS incubation of the complexes was chosen In order to access the effects of physiological concentrations of salt in particle stability, thus giving us a more approximated information on the size of particles when in an extracellular environment. DLS analysis returns results in intensity, which unfortunately has no clear conversion to nanoparticle (NP) population numbers. A single larger particle may yield higher intensity than several smaller ones, so the analysis curve gives much more weight to aggregates than individual NP. Not only must this be taken into account during the interpretation of the results, but also that single particles are closer to the detection level, so they may fail to be reported.

Small and well-distributed nanoparticles would be ideal for the intended purpose, *i.e.* cellular transfection, since internalization is dependent on low particle size[94, 95] and broad diameter distribution could lead to unexpected and/or unstable results. However, since this study focuses on chitosan derivatives, which are likely to aggregate[92], some variability was expected. The chosen N/P ratios were selected in order to assess whether great shifts in TMC concentration would have a significant impact on nanoparticle size. Also N/P 5 was selected taking into consideration that in the gel retention assay (PAGE), for both unmodified and modified TMCs, it is the lowest ratio with considerable interactions between the polymer and the AONs. As for N/P 80 it corresponds to the highest ratio used later for the *in vitro* cell transfection assays, since even higher ratios were already observed before to give high cell toxicity, especially for hydrophobically modified TMCs (previous work from the lab).

Unmodified TMC produces larger particles, especially at N/P 80, probably due to extensive aggregation (fig. 15). Hydrophobically-modified TMC, on the other hand, make smaller particles, in the range of 100-200 nm even at higher N/P ratios, which has been referred in the literature as an optimal diameter for cellular internalization[94, 96]. There is an overall high polydispersity index (PdI), which usually relates to a broad distribution of nanoparticle size.

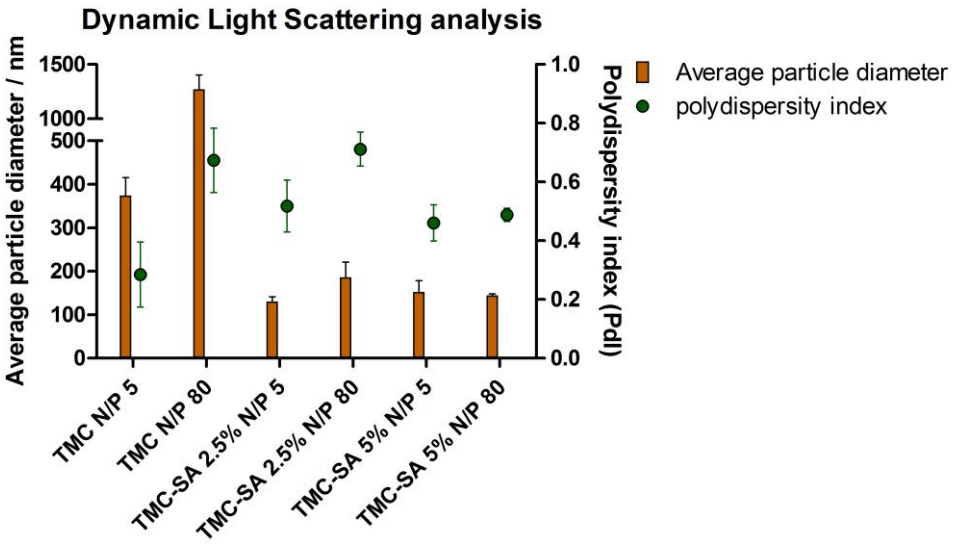

Figure 15 – **Dynamic Light Scattering analysis of unmodified, 2.5% and 5% stearic acid-modified TMC.** The high polydispersity index refers to a broad particle diameter distribution. The tendency for aggregation is lower in hydrophically modified-TMC than in the original biomaterial.

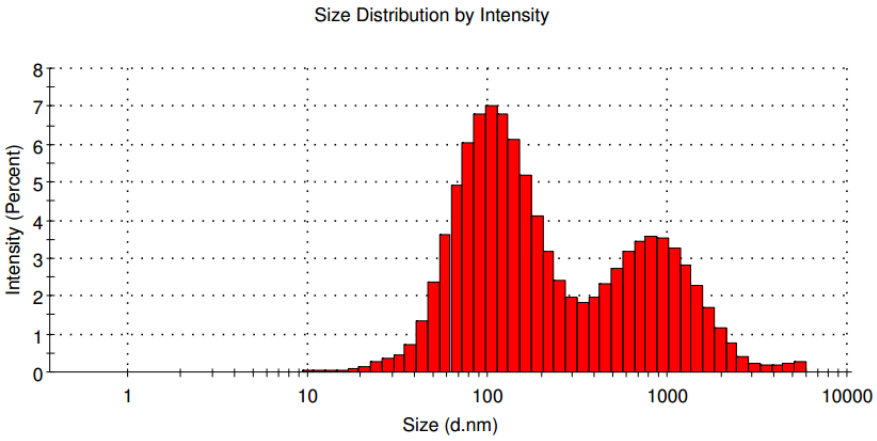

Figure 16 – **Typycal Dynamic Light Scattering analysis profile for TMC-SA 5% at N/P 80.** Although the example of 5%

SA-TMC at N/P80 was used, similar profiles were observed for other N/P ratios. Not all of the high PdI reported values are associated to broad nanoparticle size curves; in some cases, a bimodal distribution is responsible for it.

In some of the analyzed samples, however, the high PdI is representative of a bimodal distribution, as exemplified in fig. 16 with TMC-SA 5% at N/P 80. The left peak is associated with individual nanoparticles, whereas the right peak relates to aggregates. As referred before, DLS analysis yields results in intensity, which is associated to the mode of data acquisition; larger particles produce higher intensity than a similar number of smaller ones. So, despite not being possible to determine an objective translation from intensity into nanoparticle numbers, the percentage of aggregated particles is expected to be much lower than the percentage of particles in suspension. In other cases, there is a significant peak at around 1nm, which although does not offer any relevant information, influences the PdI determination (data not shown). It is expected to be an artifact, possibly derived from the high glucose concentration in the buffer solution.

After dehydration and negative staining with uranyl acetate, several samples were submitted to Transmission Electron Microscopy (TEM) analysis. Dehydration was expected to have an impact on nanoparticle shape, diameter and stability, as it may lead to NP collapse, aggregation or disruption of the original shape. The high PdI reported in the DLS analyses was an indicative of putative nanoparticle instability, which was expected as well in the TEM pictures. Indeed, most of the tested samples yielded pictures with no nanoparticles, probably due to their complete disruption.

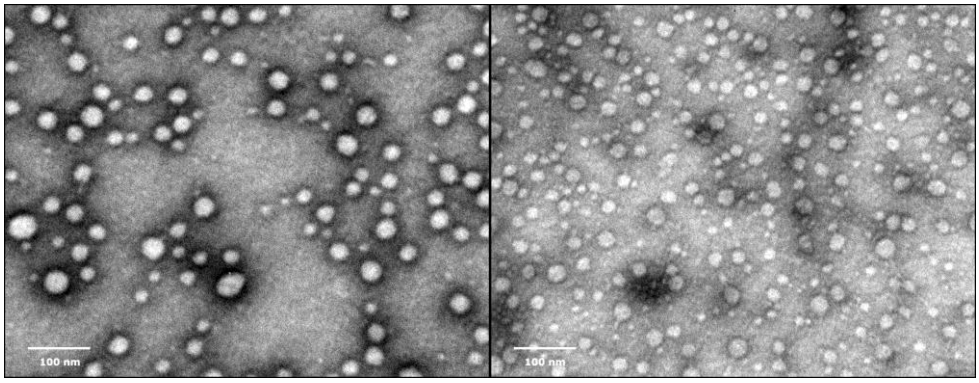

Figure 17 – **Transmission electron microscopy images of 5%-SA TMC at N/P 2 (left) and N/P 10 (right).** The regular spherical shape of the nanoparticles and the slight variance in diameter are according to expected.

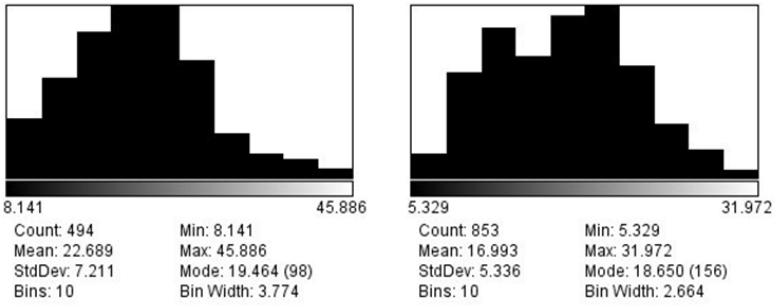

Figure 18 – **Histograms of particle size distribution of 5%-SA TMC at N/P 2 (left) and N/P 10 (right) produced from manual annotations made with the Fiji software[97].** Nanoparticle diameter was manually annotated from TEM pictures in order to assess its distribution. The X axis represents particle diameter in nm. Each column has a width of 3.774 nm or 2.664 nm respectively for N/P 2 and N/P 10.

TMC-SA 5% was successfully analyzed by TEM at N/P 2 and 10 (fig. 17). As expected, the nanoparticles had a regular spherical shape, with some variance in diameter, concordant with the PdI from the previous DLS analyses. No aggregates were observed, and the diameter was, as expected, much lower than observed by DLS method.

Manual annotations of nanoparticle diameter (fig. 18) were made using the Fiji software[97], in order to assess its distribution and compare it to DLS analyses. With quantified results, the broad size distribution is more obvious. Particle count was high (494 and 853 for N/P 2 and 10, respectively), in an attempt to produce a more robust analysis. However, it must be taken into account that most of the analyzed samples reported an unstable behavior and that dried samples are expected to have much lower diameter than hydrated, suspended particles. DLS analyses are much more reliable in diameter determination and TEM should be preferably used for shape analysis, although it also reflects the broad size distribution of the formed particles.

In vitro transfection properties of TMC

Using a reporter system that determines transfection efficiency of a specific splice-correction AON, a Luciferase assay was designed. Functional luciferase protein levels, which are exclusively dependent on efficient AON transfection, were determined by analyzing the emitted luminescence that follows substrate addition. Untreated cells were used as a negative control and reference for fold increase calculations. A free oligonucleotide sample was also included in the analysis, which produced no changes in Luciferase expression levels. The samples were analyzed at 48h since the previous analyses determined that at 24h there was very high endosomal retention; furthermore, while the previous analysis assessed internalization, functional studies require additional time for AON to have its activity.

Lipofectamine 2000, a commercial transfection reagent, was used as a positive control, since it efficiently transfects AON into HeLa cells. Two lipofectamine samples were tested, one at the same AON concentration as the remaining samples (0.3 µM), and another at a lower AON concentration (0.1 µM). These conditions yielded high Luciferase expression levels, 50 and 10 times the Relative Luminiscence Units (RLU) of the negative control, respectively, although cell viability was severely affected as seen by Optical Light Microscopy.

The three biomaterials under study were tested at several N/P ratios. Up until N/P 40, no efficient AON transfection is reported (fig. 19), since functional luciferase levels are similar to the negative (Untreated) control. Furthermore, neither unmodified TMC nor 5% SA TMC were able to transfect HeLa cells at N/P 80. 2.5% SA TMC yielded an increase of Luciferase expression of approximately 5 times the untreated control at those N/P ratios, but with a high standard deviation. This may be representative of high endosomal retention at 48h incubation.

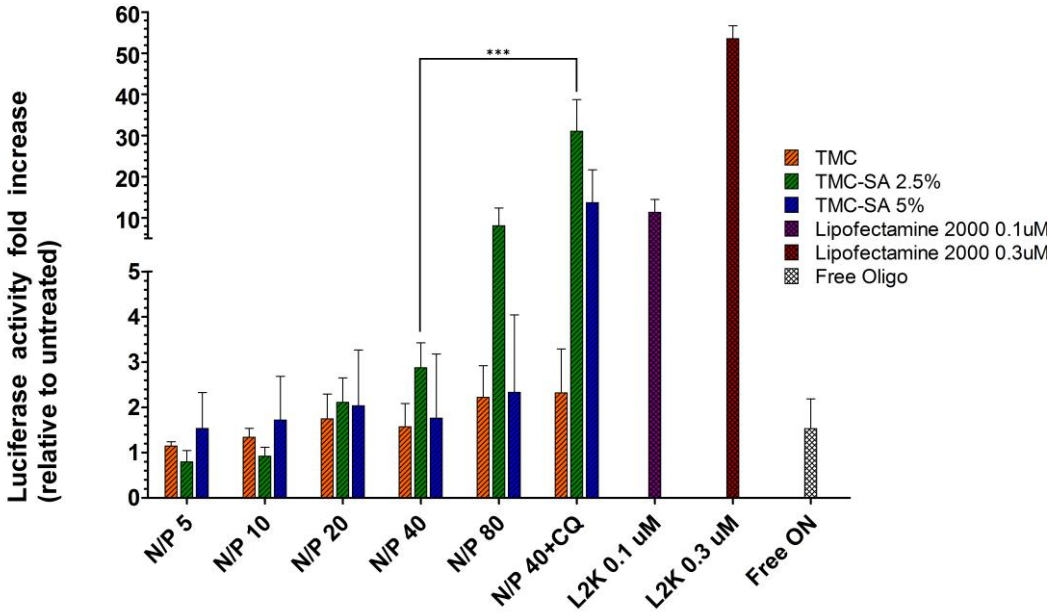

Figure 19 – **-Luminiscence levels, relative to the untreated control, of the Luciferase transfection assay.** Lipofectamine 2000, a commercial transfection reagent, was used as a control both with the same AON concentration as the remaining samples and with 1/3 of that concentration (0.3 and 0.1 µM, respectively). The difference between TMC-SA 2.5% at N/P 40 treated with CQ and TMC-SA 2.5% at N/P 40 is statistically significant (***p<0.001), although the equivalent comparisons for the untreated TMC and the TMC-SA 5% are not statistically significant.

In order to confirm that hypothesis, addition of chloroquine (CQ) was tested at N/P 40. CQ is an endosomal escape-inducing drug, with great buffering properties[63, 98]. When present in

endosomes, *e.g.* co-internalized with AON, it slows down the acidification while increasing the osmotic pressure, eventually leading to its rupture. Seeing that the levels of Luciferase from CQ-treated samples were approximately 10x higher than N/P 40 (with statistical difference of $p<0.001$ according with Tukey's test of one way analysis of variance), we can conclude that transfection with hydrophobically-modified TMC is hindered by high endosomal retention. Unmodified TMC samples, on the other hand, were unaffected by CQ addition, *i.e.* there was no endosomal retention; the low transfection levels are more likely due to nanoparticle instability and aggregation that limits cellular interaction. CQ treatments resulted in some cytotoxicity, observed by Optical Light Microscopy, although still significantly lower than lipofectamine.

TMC-SA 2.5% samples yielded higher luciferase levels than TMC-SA 5%, although the previous analyses suggest that internalization is similar for both biomaterials. The lower transfection properties of TMC-SA 5% are probably due to lower AON release from TMC-AON interaction. While AON binding properties were similar for both hydrophobically modified biomaterials in terms of association, that is not necessarily the case for complex dissociation. The latter is crucial for attaining efficient transfection, since AON are dependent on being released for exerting their function. Thus, TMC-SA 5% at N/P 40 possibly produces such strong interaction with AON that it prevents their release after entering the cell, yielding lower transfection efficiency than TMC-SA 2.5%.

For better understanding the results of transfection efficiency we decided to study the cellular binding properties of TMC-AON complexes using fluorescently labeled AON (Cy5-AON). Flow cytometry was thus used. The washing step of the flow cytometry protocol does not ensure complete removal of membrane-bound AON, but most of the remaining oligos are expected to be internalized. Even though free oligonucleotides have some binding properties themselves, complexation with TMC was expected to have a great impact. FACS based methods are not a reliable way to determine cellular localization of internalized, labeled AON, since the latter may be retained in endosomes or free in the cytosol or nucleus.

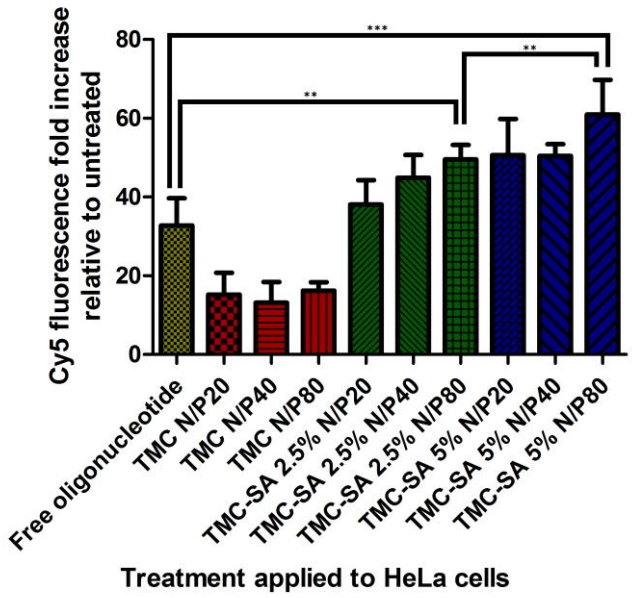

Figure 20 – **Geometric mean of the fluorescence levels of TMC-treated samples, determined by flow cytometry analysis.** HeLa cells were treated with Cy5-labeled AON and TMC in different concentrations, in triplicate. The low fluorescence levels in the unmodified TMC-treated samples are likely to derive from the aggregation properties of the biomaterial. The higher levels associated to the hydrophobically-modified TMC are indicative that the stearic acid modification is effective in stimulating cellular binding. The differences in fluorescence from 2.5% SA TMC at N/P 80 to both the free oligo control and 5% SA-TMC at N/P 80 are statistically significant (**p<0.01), as well as the difference between 5% SA TMC at N/P 80 and the free oligo control (***p<0.001).

Free ON samples have close to 35x the fluorescence levels of the non treated control, yet unmodified TMC samples have approximately half of those levels (fig. 20). Aggregation properties as seen in the DLS analyses are potentially responsible for lower cell membrane binding and internalization, since large particles are internalized with more difficulty than smaller ones. Changes in N/P ratios seem to have no impact on cellular binding of unmodified TMC nanoparticles. 2.5% and 5%-SA TMC samples, on the other hand, show higher fluorescence levels that escalate with the rise of the N/P ratio. These results are concordant to what was expected, *i.e.* stearic acid modification is successful in improving not only AON binding properties, but also cellular binding properties as well.

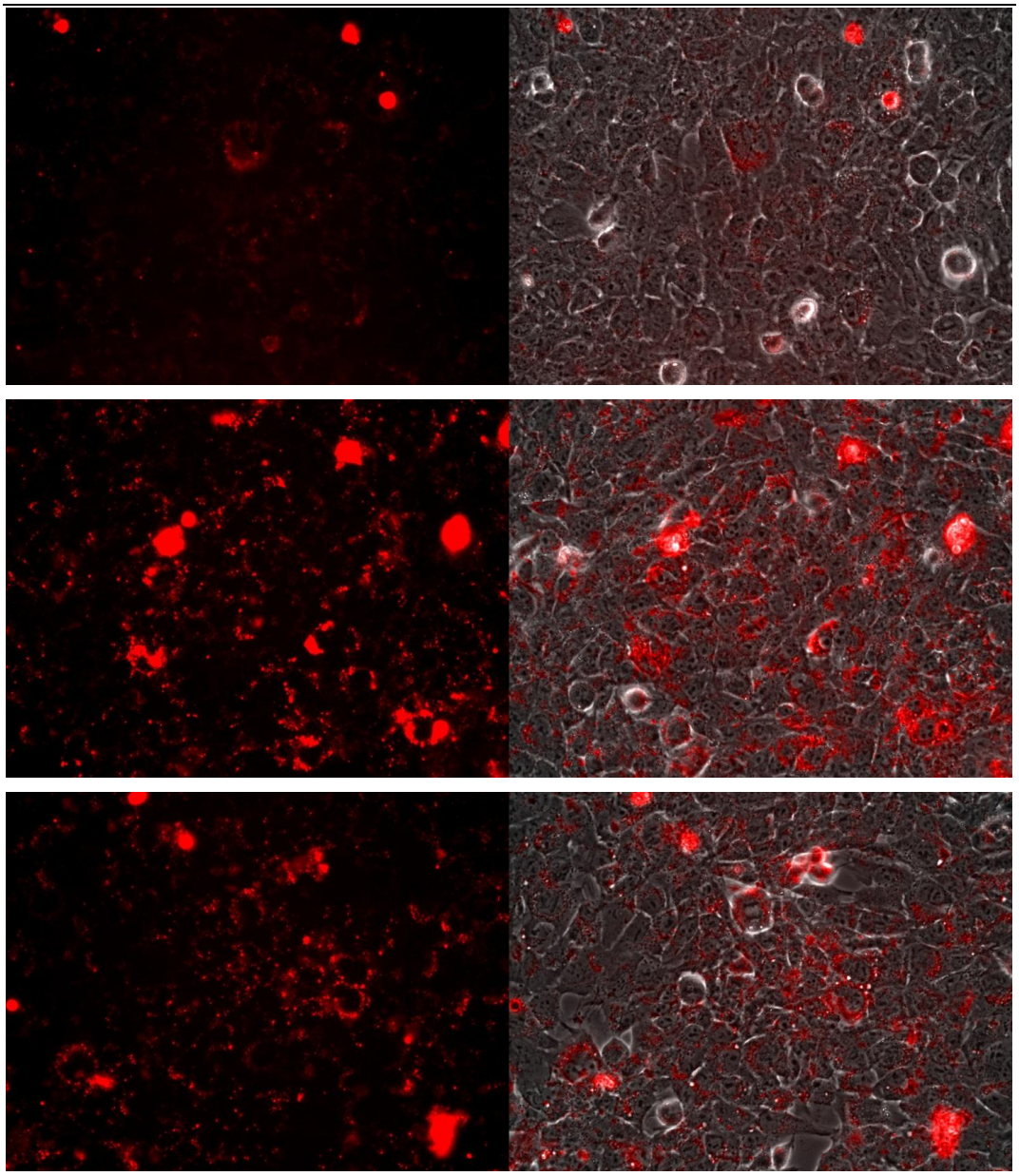

Figure 21 – **Fluorescence microscopy image of HeLa cells treated with TMC at N/P 80, TMC-SA 2.5% at N/P 40 and TMC-SA 5% at N/P 40(from top to bottom).** Fluorescence image (left); fluorescence and brightfield merge image (right). With TMC, the Cy5-labeled is mainly localized in vesicle-like structures (possibly endosomes/lysosomes), pictured by an abundance of granules close to the nucleus. A similar effect is observed in TMC-SA samples, although at higher fluorescence intensity.

Fluorescence microscopy complemented the data from the flow cytometry studies. While the latter yielded no information regarding the cellular localization of the fluorescent AON, the former allows identification of the oligo localization, although it does not enable a quantitative analysis. A

combinatorial approach of flow cytometry and fluorescence microscopy provides a better view of the cell delivery process.

This technique is capable of determining the cellular localization of fluorochrome-labeled AON. Important information may be gathered by analyzing fluorescence images, *e.g.* whether the oligonucleotides were not internalized or rather were stopped at endosomes. According to Lorenz[89, 90] *et al*, efficient transfection of phosphorothioate-modified AON is confirmed by a diffuse intranuclear staining due to a tendency for migration and accumulation of oligonucleotides in the nucleus. The microscopy pictures were taken at identical exposure times.

Unmodified TMC is unsuccessful at transfecting HeLa cells, even at N/P 80 (fig. 21). Some cells are brightly stained, but they are likely senescent and thus much more permeable. The remaining cells are faintly stained, with AON limited to vesicle like structures, possibly endosomes/lysosomes. Transfection with TMC-SA 2.5% at N/P 40 seems to result mainly in endosomal staining, although to a much larger extent. No nuclear staining was reported, but it must be kept in mind that the fluorescence microscopy analysis was done at 24h incubation, *i.e.* longer incubation could enable efficient transfection and nuclear staining. TMC-SA 5% at N/P 40 yielded similar results, *i.e.* abundance of epinuclear, granular staining and no diffuse intranuclear staining. The extensive endosomal retention may be addressed by specific approaches, *e.g.* buffering moieties, resulting in the sponge effect, or endosomal escape-inducing drugs. Nonetheless, these are results from short incubation, and longer intervals may support better transfection.

The hydrophobic modification of TMC is effective in stimulating the uptake of TMC-AON complexes. Flow cytometry results are thus confirmed, since internalization is quite higher in the modified TMC samples.

Neither Lipofectamine nor CQ are suitable for *in vivo* applications due to their cytotoxic profiles. They are useful for *in vitro*, theoretical studies, but other alternatives should be sought to increase the transfection efficiency of the complexes under test. The positive effects of the introduction of hydrophobic moieties were again confirmed, although transfection efficiency is still quite modest compared to the commercial reagent control.

Discussion and Future Directions

The antisense oligonucleotides sequences under test were successful in downregulating transcript levels, although there was high variability in the results that hindered comparative analysis. Target RNA downregulation seemed to be affected by transfection-associated toxicity or due to AON toxicity itself, thus new transfection methods should be evaluated or sequences redesigned. Any of the tested sequences is expected to efficiently deplete target RNA levels, provided that transfection is successful. Additional RT-PCR analyses are planned to confirm these results. AON chemistry was not optimized and more detailed analysis with LNA is under consideration.

Vector development was also successful regarding the polymer modification under test. Not only hydrophobically-modified TMC was more stable at physiological salt and pH conditions than the unmodified TMC, which was victim to a much more extended aggregation, but was also able to bind AON almost completely at N/P 3 and yield nanoparticles of about 150 nm, which is an adequate size for efficient uptake. Moreover, AON binding properties were enhanced beyond the requirement of lower N/P for efficient retention, since the interaction was more resistant to electrostatic shielding from high ionic strength and to nucleic acid binding dye destabilization by AON binding competition. The biomaterials form a loose particle structure that is induced by an increase on the N/P ratio or adding a hydrophobic substituent, possibly leading to a micelle-like structure that exposes most TMC-bound AON to the solvent and nucleic acid binding dyes. Buffer conditions are supposed to efficiently mimic physiological conditions, especially regarding pH and osmolarity, since complex properties were unchanged during *in vitro* analyses.

TMC transfection properties were compared with a commercial reagent, having had a lower yield. However, none of the N/P ratios tested presented obvious signs of cytotoxicity under Optical Light Microscopy, while Lipofectamine led to great cytotoxic effects. TMC, contrary to commercial reagents, is expected to be suitable for *in vivo* experiments. The issue of low transfection may be addressed by increasing nanoparticle concentration, reducing size distribution (*e.g.* by filtering or PEGylation) or by further chemical modifications. Chloroquine modification, for example, could increase the polymer buffering properties and trigger higher endosomal release, thus overcoming one of the greatest obstacles we found while attempting to transfect cells with TMC and TMC-SA.

Acknowledgments

This study was conducted in the context of the project “Characterization of Cell-intrinsic axonal regeneration determinants and their use to promote repair after CNS injury”, funded by grant HMSP-ICT/0020/2010 from FCT (Fundação para a Ciência e Tecnologia). Other team members were involved in overlapping subjects, having been crucial to the reported work, *e.g.* synthesis and characterization of hydrophobically-modified chitosan, characterization of the molecular targets (RhoA and GSK3β). The project is planned to progress with *in vivo* on animal models analysis of the tested AON-TMC complexes.

The author would like to thank his supervisors, Pedro Moreno and Ana Paula Pêgo, for the valuable support throughout the entire length of this study, to the remaining INEB members, which were very helpful as well, and to FCT for funding the project.

Bibliography

1. Abu-Rub, M., et al., *Spinal cord injury in vitro: modelling axon growth inhbition.* Drug Discovery Today, 2010. **15**(11/12): p. 436-443.
2. Rowland, J., et al., *Current status of acute spinal cord injury pathophysiology and emerging therapies: promise on the horizon.* Neurosurgical Focus, 2008. **25**(5): p. 1-17.
3. Kubo, T., et al., *The therapeutic effects of Rho-ROCK inhibitors on CNS disorders.* Therapeutics and Clinical Risk Management, 2008. **4**(3): p. 605-615.
4. Filbin, M., *Myelin-associated inhibitors of axonal regeneration in the adult mammalian CNS.* Nature Reviews Neuroscience, 2003. **4**: p. 1-11.
5. Busch, S. and J. Silver, *The role of extracellular matrix in CNS regeneration.* Current Opinion in Neurobiology, 2007. **17**: p. 120-127.
6. King, R. and P. Newmark, *The cell biology of regeneration.* Journal of Cell Biology, 2012. **196**(5): p. 553-562.
7. Bely, A., *Evolutionary Loss of Animal Regeneration: Pattern and Process.* Integrative & Comparative Biology, 2010. **50**(4): p. 515-527.
8. McKerracher, L. and M. Winton, *Nogo on the Go.* Neuron, 2002. **36**: p. 345-348.
9. Yu, P., et al., *DNA vaccine against NgR promotes functional recovery after spinal cord injury in adult rats.* Brain Research, 2007. **1147**: p. 66-76.
10. Ahmed, Z., et al., *Disinhibition of neurotrophin-induced dorsal root ganglion cell neurite outgrowth on CNS myelin by siRNA-mediated knockdown of NgR, $p75^{NTR}$ and Rho-A.* Molecular and Cellular Neuroscience, 2005. **28**(3): p. 509-523.
11. Yamashita, T., et al., *Rho/Rho-kinase as potential therapeutic targets for CNS injury.* Gene Therapy and Molecular Biology, 2005. **9**: p. 265-268.
12. Sharma, K., M. Selzer, and S. Li, *Scar-mediated inhibition and CSPG receptors in the CNS.* Experimental Neurology, 2012. **237**: p. 370-378.
13. David, S. and S. Lacroix, *Molecular Approaches to Spinal Cord Repair.* Annual Review of Neurosciences, 2003. **26**: p. 411-440.
14. Ahmed, Z., M. Berry, and A. Logan, *ROCK inhibition promotes adult retinal ganglion cell neurite outgrowth only in the presence of growth promoting factors.* Molecular and Cellular Neuroscience, 2009. **42**: p. 128-133.
15. Sugate, E., et al., *Optimisation of siRNA-mediated RhoA silencing in neuronal cultures.* Molecular and Cellular Neuroscience, 2009. **40**: p. 451462.
16. Cheng, C., et al., *Activated RHOA and peripheral axon regeneration.* Experimental Neurology, 2008. **212**: p. 358-369.
17. Tang, A., W. Campbell, and K. Nithipatikom, *ROCK1 feedback regulation of the upstream small GTPase RhoA.* Cellular Signaling, 2012. **24**(7): p. 1375-1380.
18. Miron, I., *Functional consequences of complete GSK-3 ablation in mouse embryonic fibroblasts,* in *Graduate Department of Medical Biophysics*2008, University of Toronto.
19. Doble, B. and J. Woodgett, *GSK-3: tricks of the trade for a multi-tasking kinase.* Journal of Cell Science, 2003. **116**: p. 1175-1186.
20. ter Haar, E., et al., *Structure of GSK3b reveals a primed phosphorylation mechanism.* Nature Structural Biology, 2001. **8**(7): p. 593-596.
21. Sayas, L., J. Avila, and F. Wandosell, *Glycogen synthase kinase-3 is activated in neuronal cells by Ga12 and Ga13 by Rho-independent and Rho-dependent mechanisms.* Journal of Neuroscience, 2002. **22**(16): p. 6863-6875.
22. Hur, E.-M., et al., *GSK3 controls axon growth via CLASP-mediated regulation of growth cone microtubules.* Genes & Development, 2011. **25**(1968-1981).
23. Azim, K. and A. Butt, *GSK3b negatively regulates oligodendrocyte differentiation and myelination in vivo.* Glia, 2011. **59**(4): p. 540-533.
24. Seira, O., et al., *Neurites regrowth of cortical neurons by GSK3b, inhibition independently of Nogo receptor 1.* Journal of Neurochemistry, 2010. **113**: p. 1644-1658.
25. Alabed, Y., et al., *GSK3b Regulates Myelin-Dependent Axon Outgrowth Inhibition through CRMP4.* Journal of Neuroscience, 2010. **30**(16): p. 5635-5643.
26. Spencer, T., et al., *New roles for old proteins in adult CNS axonal regeneration.* Current Opinion in Neurobiology, 2003. **13**: p. 133-139.
27. Hu, F. and S. Strittmatter, *Regulating Axonal Growth within the Postnatal Central Nervous System.* Seminars in

Perinatology, 2004. **28**: p. 371-378.
28. Winton, M., et al., *Characterization of new cell permeable c3-like proteins that inactivate Rho and stimulate neurite outgrowth on inhibitory substrates.* Journal of Biological Chemistry, 2002. **277**: p. 32820-32829.
29. Mittnacht, U., et al., *Chitosan/siRNA nanoparticles biofunctionalize nerve implants and enable neurite outgrowth.* Nano Letters, 2010. **10**: p. 3933-3939.
30. Cadotte, D. and M. Fehlings, *Spinal Cord Injury: A Systematic Review of Current Treatment Options.* Clinical Orthopaedics and Related Research, 2011. **469**: p. 732-741.
31. Baba, H., et al., *Protective effects of cold spinoplegia with fasudil against ischemic spinal cord injury in rabbits.* Journal of Vascular Surgery, 2010. **51**(2): p. 445-452.
32. Sung, J.-K., et al., *A possible role of RhoA/Rho-kinase in experimental cord injury in rat.* Brain Research, 2003. **959**(1): p. 29-38.
33. Furuya, T., et al., *Treatment of rat spinal cord injury with a Rho-kinase inhibitor and bone marrow stromal cell transplantation.* Brain Research, 2009. **1295**: p. 192-202.
34. Chiu, C.-T. and D.-M. Chuang, *Molecular actions and therapeutic potential of lithium in preclinical and clinical studies of CNS disorders.* Pharmacology & Therapeutics, 2010. **128**(2): p. 281-304.
35. Skaper, S., S. Moore, and F. Walsh, *Cell signaling cascades regulating neuronal growth-promoting and inhibitory cues.* Progress in Neurobiology, 2001. **65**: p. 593-608.
36. Jaeger, A., *Lithium.* Medicine, 2012. **40**(3): p. 131-132.
37. Fire, A., et al., *Potent and specific genetic interference by double-stranded RNA in Caenorhabditis elegans.* Nature, 1998. **391**(6669): p. 806-11.
38. Bennet, F. and E. Swayze, *RNA Targeting Therapeutics: Molecular Mechanisms of Antisense Oligonucleotides as a Therapeutic Platform.* Annual Review of Pharmacology and Toxicology, 2010. **50**: p. 259-293.
39. Couvreur, P. and C. Malvy, *Pharmaceutical Aspects of Oligonucleotides*, ed. T.F. Group2005.
40. Kim, T.H., et al., *Conserved functional characteristics of the PIWI family members in chicken germ cell lineage.* Theriogenology, 2012. **78**: p. 1948-1959.
41. Parker, J., et al., *Enhancement of the Seed-Target Recognition Step in RNA silencing byb a PIWI/MID Domain Protein.* Molecular Cell, 2009. **33**: p. 204-214.
42. Chan, J., S. Lim, and F. Wong, *Antisense oligonucleotides: From design to therapeutic application.* Clinical and Experimental Pharmacology and Physiology, 2006. **33**: p. 533-540.
43. Crooke, S., *Antisense Drug Technology*, ed. T.F. Group2008.
44. Smith, L., et al., *Rational selection of antisense oligonucleotide sequences.* European Journal of Pharmaceutical Sciences, 2000. **11**(3): p. 191-198.
45. Sazani, P., M. Vacek, and R. Kole, *Short-term and long-term modulation of gene expression by antisense therapeutics.* Current Opinion in Biotechnology, 2002. **13**(5): p. 468-472.
46. Petros, A., E. Olejniczack, and S. Fesik, *Structural biology of the Bcl-2 family of proteins.* Biochimica et Biophysica Acta - Molecular Cell Research, 2004. **1644**(2-3): p. 83-94.
47. Kole, R., A. Krainer, and S. Altman, *RNA therapeutics: beyond RNA interference and antisense oligonucleotides.* Nature Reviews, 2012. **11**: p. 125-140.
48. Rando, T., *Oligonucleotide-mediated gene therapy for muscular dystrophies.* Neuromuscular Disorders, 2002. **12**(Supplement): p. S55-S60.
49. Rando, T., *Non-viral therapy for Duchenne muscular dystrophy: Progress and challenges.* Biochimica et Biophysica Acta - Molecular Basis of Disease, 2007. **1722**(2): p. 263-271.
50. McClorey, G., S. Fletcher, and S. Wilton, *Splicing intervention for Duchenne muscular dystrophy.* Current Opinion in Pharmacology, 2005. **5**(5): p. 529-534.
51. Gebski, B., et al., *Terminal antisense oligonucleotide modifications can enhance induced exon skipping.* Neuromuscular Disorders, 2005. **15**(9-10): p. 622-629.
52. Crooke, S., *Molecular mechanisms of action of antisense drugs.* Biochimica et Biophysica Acta, 1999. **1489**: p. 31-44.
53. Zhang, P., et al., *Synergistic down-regulation of telomerase by all-trans retinoic acid and antisense oligonucleotide in oral squamous cell carcinoma cell line (Tca8113).* Oral Oncology, 2005. **41**: p. 909-915.
54. Tarkanyi, I., et al., *Inhibition of human telomerase by oligonucleotide chimeras, composed of an antisens moiety and a chemically modified homo-oligonucleotide.* FEBS Letters, 2005. **579**: p. 1411-1416.
55. Han, M., et al., *In vitro and in vivo tumor suppressive activity induced by human telomerase transcriptase-targeting antisense oligonucleotides mediated by cationic liposomes.* Journal of Bioscience and Bioengineering, 2008. **106**(3): p. 243-247.
56. Bennet, F., *Antisense Oligonucleotides: Is the Glass Half Full or Half Empty?* Biochemical Pharmacology, 1998. **55**:

p. 9-19.
57. Cook, P., *Antisense Medicinal Chemistry.* Handbook of Experimental Pharmacology, 1998. **131**: p. 51-101.
58. Dias, N. and C.A. Stein, *Antisense oligonucleotides: Basic concepts and mechanisms.* Molecular Cancer Therapy, 2002. **1**: p. 347-355.
59. Phillips, I., *Antisense Therapeutics*, ed. H.P. Inc.2005.
60. Geary, R., *Antisense oligonucleotide pharmacokinetics and metabolism.* Expert Opinion on Drug Metabolism ^ Toxicology, 2009. **5**(4): p. 381-391.
61. Rudin, C., et al., *Phase I trial of ISIS 5132, an antisense oligonucleotide inhibitor of c-raf-1, administred by 24-hour weekly infusion to patients with advanced cancer.* Clinical Cancer Research, 2001. **7**: p. 1214-1220.
62. Chen, B. and M. Bartlett, *A one-step solid phase extraction method for bioanalysis of a phosphoriothioate oligonucleotide and its 3' n-1 metabolite from rat plasma by uHPLC-MS/MS.* American Association of Pharmaceutical Scientists, 2012. **14**(4): p. 772-780.
63. Kim, T.-H., et al., *Chemical modification of chitosan as a gene carrier in vitro and in vivo.* Progress in Polymer Science, 2007. **32**: p. 726-753.
64. Liu, W. and K. Yao, *Chitosan and its derivatives - a promising non-viral vector for gene transfection.* Journal of Controlled Release, 2002. **83**: p. 1-11.
65. Mao, S., W. Sun, and T. Kissel, *Chitosan-based formulations for delivery of DNA and siRNA.* Advanced Drug Delivery Reviews, 2010. **62**: p. 12-27.
66. Moreno, P., *Nucleic Acids in Gene Delivery and Gene Regulation*, in *Department of Laboratory Medicine*2011, Karolinska Institutet: Stockholm, Sweden. p. 83.
67. Bolhassani, A., *Potential efficacy of cell-penetrating peptides for nucleic acid drug delivery in cancer.* Biochimica et Biophysica Acta, 2011. **1816**: p. 232-246.
68. Milletti, F., *Cell-penetrating peptides: class, origin and current landscape.* Drug Discovery Today, 2012. **17**(15-16): p. 850-860.
69. Ziegler, A., *Thermodinamic studies and binding mechanisms of cell-penetrating peptides with lipids and glycosaminoglycans.* Advanced Drug Delivery Reviews, 2008. **60**: p. 580-597.
70. Pujals, S., et al., *Mechanistic aspects of CPP-mediated intracellular drug delivery: relevance of CPP self-assembly.* Biochimica et Biophysica Acta, 2006. **1758**: p. 264-279.
71. Brooks, N., et al., *Cell-penetrating peptides: Application in vaccine delivery.* Biochimica et Biophysica Acta, 2010. **1805**: p. 25-34.
72. Pasut, G., M. Sergi, and F. Veronese, *Anti-cancer PEG-enzymes: 30 years old, but still a current approach.* Advanced Drug Delivery Reviews, 2008. **60**(1): p. 69-78.
73. Ahn, H., et al., *Polyethylenimine-mediated gene delivery into human adipose derived stem cells.* Biomaterials, 2008. **29**: p. 2415-2422.
74. Zheng, F., et al., *Chitosan nanoparticle as gene therapy vector via gastrointestinal mucosa administration: Results of an in vitro and in vivo study.* Life Sciences, 2007. **80**(4): p. 388-396.
75. Gao, J.-Q., et al., *Gene-carried chitosan-linked-PEI induced high gene transfection efficiency with low toxicity and significant tumor-repressive activity.* International Journal of Pharmaceutics, 2010. **387**(1-2): p. 286-294.
76. Jiang, H.-L., et al., *Chitosan-graft-spermidine as a gene carrier in vitro and in vivo.* European Journal of Pharmaceutics and Biopharmaceutics, 2011. **77**(1): p. 36-42.
77. Moreira, C., et al., *Improving chitosan-mediated gene transfer by the introduction of intracellular buffering moieties into the chitosan backbone.* Acta Biomaterialia, 2009. **5**(8): p. 2995-3006.
78. MacLaughlin, F., et al., *Chitosan and depolymerized chitosan oligomers as condensing carriers for in vivo plasmid delivery.* Journal of Controlled Release, 1998. **56**: p. 259-272.
79. Köping-Höggård, M., et al., *Improved chitosan-mediated gene delivery based on easily dissociated chitosan polyplexes of highly defined chitosan oligomers.* Gene Therapy, 2004. **11**: p. 1441-1452.
80. Li, J., J. Revol, and R. Marchessault, *Rheological properties of aqueous suspensions of chitin crystallites.* Journal of Colloid Interface Science, 1996. **183**(2): p. 365-373.
81. Mourya, V. and N. Inamdar, *Trimethyl chitosan and its application in drug delivery.* Journal of Materials Science, 2009. **20**: p. 1057-1079.
82. Oliveira, H., et al., *Chitosan-based gene delivery vectors targeted to the peripheral nervous system.* Journal of Biomedical Materials Research, 2010. **95A**(3): p. 801-810.
83. Liu, Z., et al., *Hydrophobic modifications of cationic polymers for gene delivery.* Progress in Polymer Science, 2010. **35**: p. 1144-1162.
84. Saul, J., et al., *Delivery of non-viral gene carriers from sphere-templated fibrin scaffolds for sustained transgene expression.* Biomaterials, 2007. **28**(31): p. 4705-4716.

85. Astriab-Fisher, A., et al., *Increased uptake of antisense oligonucleotides by delivery as double stranded complexes.* Biochemical Pharmacology, 2004. **68**: p. 403-407.
86. Mintzer, M. and E. Simanek, *Nonviral Vectors for Gene Delivery.* Chem. Rev., 2009. **109**: p. 259-302.
87. Ding, Y., C. Chan, and C. Lawrence, *Sfold web server for statistical folding and rational design of nucleic acids.* Nucleic Acid Research, 2004(32): p. W135-41.
88. Kang, S., M. Cho, and R. Kole, *Up-regulation of luciferase gene expression with antisense oligonucleotides: implications and applications in functional assay development.* Biochemistry, 1998. **37**(18): p. 6235-9.
89. Lorenz, P., et al., *Nucelocytoplasmatic shuttling: a novel in vitro property of antisense phosphoriotioate oligodeoxyucleotides.* Nucleic Acids Research, 2000. **28**(2): p. 582-592.
90. Lorenz, P., et al., *Phosphorotioate Antisense Oligonucleotides Induce the Formation of Nuclear Bodies.* Molecular Biology of the Cell, 1998. **9**: p. 1007-1023.
91. Uchegbu, I., et al., *Gene Transfer with Three Amphilic Glycol Chitosans - The degree of polymerisation is the main controller of transfection efficiency.* Journal of Drug Targeting, 2004. **12**(8): p. 527-539.
92. Philippova, O.E. and E.V. Korchahina, *Chitosan and its hydrophobic derivatives: preparation and aggregation in dilute aqueous solutions.* Polymer Science, 2012. **54**(7): p. 552-572.
93. Yuan, H.-Y., et al., *Stearic acid-g-chitosan polymeric micelle for oral drug delivery: in vitro transport and in vivo absorption.* Molecular Pharmaceutics, 2011. **8**(1): p. 225-238.
94. He, C., et al., *Effects of particle size and surface charge on cellular uptake and biodistribution of polymeric nanoparticles.* Biomaterials, 2010. **31**: p. 3657-3666.
95. Hu, Y., et al., *Effect of PEG conformation and particle size on the cellular uptake efficiency of nanoparticles with the HepG2 cells.* Journal of Controlled Release, 2007. **118**: p. 7-17.
96. Xu, A., et al., *A physical model for size-dependent cellular uptake of nanoparticle modified with cationic surfactants.* Internation Journal of Nanomedicine, 2012. **7**: p. 3547-3554.
97. Schindelin, J., et al., *Fiji: an open-source platform for biological-image analysis.* Nature Methods, 2012. **9**(7): p. 676-682.
98. Garcia-Chaumont, C., et al., *Delivery systems for antisense oligonucleotides.* Pharmacology & Therapeutics, 2000. **87**: p. 255-277.